

Faculty of Sciences
Department of Mathematics & Statistical Sciences

Fractional Simulations of Casson nanofluid and hybrid nanofluid flow over a vertical plate with radiation and vibration conditions.

by

Omphile Nelson Seabe
Reg. No: 13000682
BSc. Applied Mathematics, BIUST, Botswana.

A Thesis Submitted to the Faculty of Sciences in Partial Fulfilment of the Requirements for the Award of the Degree of Master of Science in Pure and Applied Mathematics of BIUST.

Supervisor:

Prof. Sachin Shaw
Department of Mathematics & Statistical Sciences,
Faculty of Sciences, BIUST
E-mail: shaws@biust.ac.bw

November 19, 2023

POSTGRADUATE SCHOOL

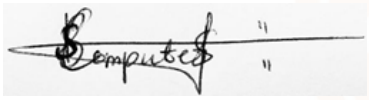
Declaration Regarding the Work and Copyright

DECLARATION REGARDING THE WORK AND COPYRIGHT

Candidate Omphile Nelson Seabe
Student ID: 13000682
Thesis Titled: Fractional Simulations of Casson nanofluid and hybrid nanofluid flow over a vertical plate with radiation and vibration conditions.

I **Omphile Nelson Seabe**, certify that the Thesis is all my own original work and that I have not obtained a degree in this University or elsewhere on the basis of any of this work.

This dissertation/thesis is copyright material protected under the Berne Convention, the Copyright and Neighbouring Rights Act, Act. No. 8 of 2000 and other international and national enactments, in that behalf, on intellectual property. It must not be reproduced by any means, in full or in part, except for short extracts in fair dealing; for researcher private study, critical scholarly review or discourse with an acknowledgement, without the written permission of the office of the Postgraduate School, on behalf of both the author and the BIUST.

Signed:  Date: 19 November 2023

Primary Supervisor Professor Sachin Shaw

I **Professor Sachin Shaw**, hereby confirm that I have inspected the above titled thesis and, to the best of my knowledge, it is based on the original work of the candidate.

Signed:  Date: 20/11/2023

Abstract

This thesis investigates the dynamics of blood nanofluid and hybrid nanofluid flow over a vertical plate using fractional calculus, with radiation and vibration conditions. Two models are presented for the simulations, using two different fractional definitions. In the first model the Prabhakar fractional derivative is applied with blood as the base fluid and Single-wall carbon nanotube (SWCNT) and Multi-wall carbon nanotubes (MWCNT) as the nanoparticles to form the nanofluids. The second model applies the Atangana-Baleanu fractional derivative, with Copper (Cu) and Aluminium Oxide (Al_2O_3) nanoparticles being used to form the hybrid nanofluid. The governing equations for the blood nanofluid and hybrid nanofluid are derived and solved using the Laplace transform technique. Numerical computation of the inverse Laplace transform was performed using the Tzou's and Zakian's algorithms. The effects of various parameters, such as the fractional orders, and nanoparticle volume fraction, on the velocity and temperature profiles are analyzed. The results show that the Prabhakar and Atangana-Baleanu fractional derivatives can effectively model the behavior of the blood nanofluid and hybrid nanofluid, and that the nanoparticle volume fraction has a significant impact on the fluid dynamics. Furthermore, the research investigates and discusses the effects of additional fluid parameters such as the Prandtl number, Grashof number, Nusselt number, and Skin friction. The effects of applied radiation and vibration is also analysed and discussed. The study concludes that the use of fractional derivatives provides a valuable tool for analyzing complex fluid dynamics problems and can be applied to a wide range of practical applications in engineering and medicine.

Dedications

Dedicated to my parents Bugalo B. Seabe and Seiphoreng J. Mogotsi,
and my brother Kitso V. Seabe.

Kea leboga batsadi bame.

Acknowledgements

Foremost, I would like to thank my supervisor, Professor Sachin Shaw, for his professional guidance throughout the course of this project. His insights, critiques, and patience have been instrumental in shaping the direction and quality of this thesis. I will forever remember his academic advise and his expertise as a motivation in my career. I have benefited greatly from his knowledge.

Furthermore, I would like to thank all the lecturers and professors who contributed to my knowledge, wisdom and expertise while studying at Botswana International University of Science and Technology (BIUST). Their broad knowledge was a great contribution towards my growing knowledge the field of mathematics.

Many thanks to the Simons Foundation for sponsoring me to do this masters degree. Their support has been essential in providing the resources and opportunities necessary for the successful completion of this degree.

Lastly, many thanks to my parents Bugalo B. Seabe and Seiphoreng J. Mogotsi, as well as my brother Kitso V. Seabe for their endless love, support, and encouragement. Their constant motivation and belief in me have been the driving force behind my academic accomplishments.

List of Symbols

B_o	Magnetic constant
B_t	Coefficient of thermal expansion
C_f	Skin friction coefficient
C_p	Specific heat
m	Particle shape factor
M	Magnetic parameter
k	Permeability constant
k^*	Mean absorption coefficient
Nu	Nusselt number
Pr	Prandtl Number
Gr	Grashof Number
q	Radiative heat flux
T	Fluid temperature
T_W	Fluid temperature on the surface
T_∞	Ambient temperature

Greek symbols

τ_w	Shear stress at the wall
ϕ	Volume fraction of the nanoparticles
ρ	Density (Kgm^{-3})
σ	Electrical conductivity
σ^*	Stefan Boltzmann constant
β	Casson nanofluid parameter
μ_B	Plastic dynamic viscosity
ν	Kinematic viscosity

Subscripts

f	Base fluid
nf	Nanofluid
hnf	Hybrid nanofluid

Abbreviations

NF	Nanofluid
HNF	Hybrid nanofluid
ABFD	Atangana - Baleanu Fractional Derivative
PBFD	Prabhakar Fractional Derivative
ILT	Inverse Laplace Transform
IC	Initial Conditions
BC	Boundary Conditions

Contents

Declaration Regarding the Work and Copyright i

Abstract ii

Dedications iv

Acknowledgements v

1 Introduction 1

1.1 Viscosity . . . 1
1.2 Newtonian and non-Newtonian fluids . . . 1
1.3 Kinematic Viscosity . . . 2
1.4 Conservation of Mass . . . 2
1.5 Conservation of Momentum . . . 3
1.6 Conservation of Energy . . . 4
1.7 Nanofluids . . . 5
1.8 Hybrid Nanofluids . . . 5
1.9 Prandtl Number . . . 5
1.10 Grashof Number . . . 6
1.11 Nusselt Number . . . 6
1.12 Skin friction coefficient . . . 6
1.13 Radiation . . . 7
1.14 Casson Fluid . . . 7
1.15 Fractional Order Derivatives . . . 7
1.15.1 Caputo fractional derivative . . . 8
1.15.2 Caputo - Fabrizio fractional derivative . . . 8
1.15.3 Atangana - Baleanu fractional derivative (ABFD) . . . 8
1.15.4 Prabhakar fractional derivative (PBFD) . . . 8
1.16 Objectives . . . 9
1.17 Thesis Outline . . . 9

2 Literature Review 11

3 Prabhakar fractional simulation of thermal Casson nanofluid flow with SWCNT and MWCNT in radiation and vibrating conditions 15

3.1 Introduction . . . 15
3.2 Mathematical Model . . . 15
3.3 Prabhakar Fractional Order . . . 18
3.4 Solution of the problem . . . 19

3.4.1 Solution of the temperature profile [Equations (3.9) and (3.12)] 19
3.4.2 Solution of the velocity profile [Equation (3.8)] 20
3.5 Numerical Results and Discussion 21
3.5.1 Comparison of Tzou and Zakian numerical schemes 21
3.5.2 Effect of fractional variables α, β and γ 22
3.5.3 Effect of Nanoparticle Volume Fraction ϕ 23
3.5.4 Effect of Radiation parameter R and Vibration 24
3.5.5 Effect of Prandtl Number Pr and Grashof Number Gr 25
3.5.6 Nusselt Number Nu and Skin friction C_f 26
3.6 Conclusions 28

4 Atangana-Baleanu fractional simulation of thermal $Cu - Al_2O_3$/Casson hybrid NF flow with radiation across an oscillating surface considering shape effects 29
4.1 Introduction 29
4.2 Mathematical Formulation 29
4.3 Atangana-Baleanu Fractional Order 33
4.4 Solution of the problem 34
4.4.1 Solution of the temperature profile [Equations (4.8) and (4.11)] 34
4.4.2 Solution of the velocity profile [Equation (4.7)] 34
4.5 Numerical Results and Discussion 35
4.5.1 Comparison of numerical schemes 35
4.5.2 Effect of fractional parameter β 37
4.5.3 Effect of Prandtl Number Pr and Magnetic Parameter M 38
4.5.4 Effect of Nanoparticle Volume Fraction ϕ 39
4.5.5 Impact of the shape of the nanoparticles 40
4.5.6 Effect of Radiation parameter R 41
4.5.7 Effect of Grashof Number Gr and Angle θ 41
4.5.8 Nusselt Number Nu and Skin Friction C_f 42
4.6 Conclusions 43

5 Conclusions & Future Scope 45
5.1 Conclusions 45
5.2 Future Scope 46

Appendix 47

A Appendix for Chapter 3 47
A.1 Values of Constants for equation 3.20 47
A.2 Solution steps of Temperature profile 47
A.3 Solution steps for Velocity Profile 49

B Appendix for Chapter 4 54
B.1 Solution steps of Temperature profile 54
B.2 Solution steps of Velocity profile 56

1. Introduction

A fluid is a substance that continually deforms (flows) when acted upon by shear stress. Fluid motion can manifest in different forms, including uniform or non-uniform flow, compressible or incompressible behavior, viscous or inviscid nature, rotational or irrotational motion, and steady or unsteady patterns. The behavior of fluids is determined by a fundamental set of essential physical conservation laws. These laws are the basis of the governing equations in fluid mechanics.

The demand for enhancing the thermal properties of heat transfer fluids has witnessed a substantial increase in the past century [1]. As a result, this has been a very active subject studied by scientists and engineers. One of the most successful ways that this has been achieved is through the use of heat transfer fluids called nanofluids (NFs) and hybrid nanofluids (HNFs).

This chapter highlights fundamental fluid conservation laws and properties, NFs and HNFs, and gives a brief introduction to fractional order calculus. Subsequently, the aims of this research will be examined.

1.1 Viscosity

Viscosity, denoted as μ, quantifies the degree of resistance a fluid exhibits against deformation due to shear or tensile stress.

1.2 Newtonian and non-Newtonian fluids

The behavior of a Newtonian fluid is characterized by the direct proportionality between the viscous stress and the rate of deformation in the flow. This property is also known as Newton's Law of Viscosity. Mathematically, this is denoted:

$$\tau \propto \left(\frac{\partial u}{\partial y}\right),$$

$$\tau = \mu \frac{\partial u}{\partial y}, \tag{1.1}$$

where τ represents the viscous shear stress, μ denotes the viscosity, and $\frac{\partial u}{\partial y}$ signifies the shear rate. If a fluid does not obey this property, then it is called a non-Newtonian fluid. In other words, non-Newtonian fluids are fluids where the velocity gradient and shear stress are not linearly proportional. This implies that the connection between shear stress and shear rate can exhibit variability depending on the fluid being analyzed. In mathematical terms, it can be

formulated as:

$$\tau \propto \left(\frac{\partial u}{\partial y}\right)^n, n \neq 1.$$

Figure (1.1) shows the behaviour of Newtonian fluids and various types of non-Newtonian fluids, with respect to shear stress and shear rate. It is important to note that blood exhibits shear-thinning flow (pseudoplastic properties).

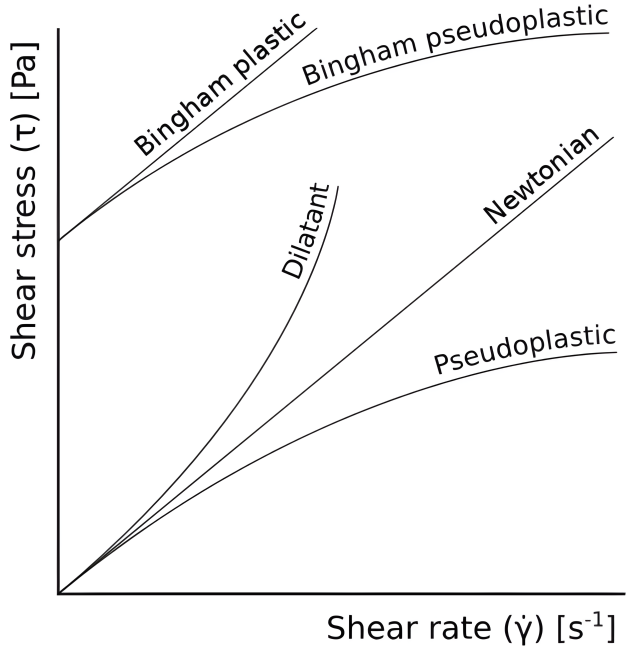


Figure 1.1: Shear stress/rate profile of Newtonian and non-Newtonian fluids [2]

1.3 Kinematic Viscosity

The quantity known as kinematic viscosity, symbolized by ν, is obtained by dividing the dynamic viscosity by the mass density. That is,

$$\nu = \frac{\mu}{\rho}. \tag{1.2}$$

1.4 Conservation of Mass

The principle of mass conservation, also referred to as continuity, posits that in a closed system, the total mass remains constant and cannot be created or destroyed. In fluid mechanics, this means that the rate at which mass enters and leaves the system are equal. This can be represented mathematically as the continuity equation in this manner:

$$\frac{\partial \rho}{\partial t} + \nabla(\rho V) = 0, \tag{1.3}$$

where the vector $V = (u, v, w)$ represents the velocity at time t. For a steady, incompressible flow, density (ρ) is constant. Hence $\frac{\partial \rho}{\partial t} = 0$. Therefore:

$$\nabla(\rho V) = 0, \tag{1.4}$$

which further simplifies to:

$$\frac{\partial u}{\partial x} + \frac{\partial v}{\partial y} + \frac{\partial w}{\partial z} = 0. \tag{1.5}$$

For a two-dimensional flow:

$$\frac{\partial u}{\partial x} + \frac{\partial v}{\partial y} = 0. \tag{1.6}$$

1.5 Conservation of Momentum

The total momentum within a closed system remains constant according to the law of conservation of momentum. The general form for the momentum equation is given as:

$$\rho \frac{dV}{dt} = \rho g - \nabla p + \nabla \tau_y. \tag{1.7}$$

The above equation can be represented in the form of Navier-Stokes equations. Figure 1.2 below shows the shear stresses in a cube control volume using the Cartesian coordinate system.

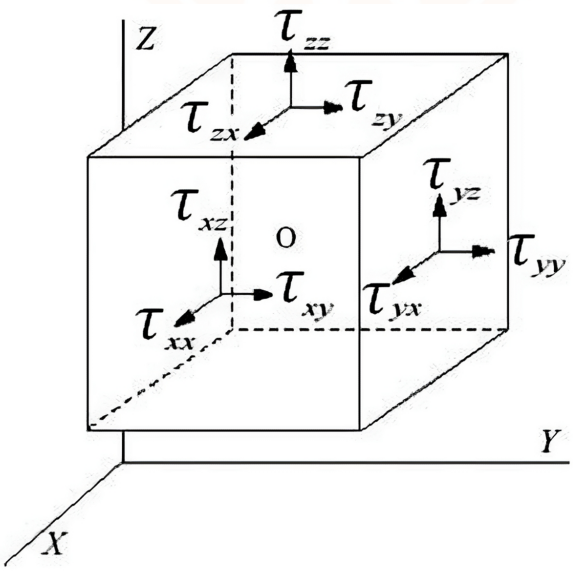


Figure 1.2: Notation for stresses [3]

The Navier-Stokes equations in the Cartesian coordinate system are given separately for the x, y, and z directions as:

$$\rho\left(\frac{\partial u}{\partial t}+u\frac{\partial u}{\partial t}+v\frac{\partial u}{\partial t}+w\frac{\partial u}{\partial t}\right)=\rho F_x+\frac{\partial p}{\partial x}-\left(\frac{\partial \tau_{xx}}{\partial x}+\frac{\partial \tau_{yx}}{\partial y}+\frac{\partial \tau_{zx}}{\partial z}\right), \tag{1.8}$$

$$\rho\left(\frac{\partial v}{\partial t}+u\frac{\partial v}{\partial t}+v\frac{\partial v}{\partial t}+w\frac{\partial v}{\partial t}\right)=\rho F_y+\frac{\partial p}{\partial y}-\left(\frac{\partial \tau_{yy}}{\partial x}+\frac{\partial \tau_{xy}}{\partial y}+\frac{\partial \tau_{zy}}{\partial z}\right), \tag{1.9}$$

$$\rho\left(\frac{\partial w}{\partial t}+u\frac{\partial w}{\partial t}+v\frac{\partial w}{\partial t}+w\frac{\partial w}{\partial t}\right)=\rho F_z+\frac{\partial p}{\partial z}-\left(\frac{\partial \tau_{zz}}{\partial x}+\frac{\partial \tau_{xz}}{\partial y}+\frac{\partial \tau_{yz}}{\partial z}\right), \tag{1.10}$$

where F_i is the body force (which includes gravitational force g), and τ_{ij} are the shear stresses. For incompressible flow, the above equations simplify to:

$$\rho\left(\frac{\partial u}{\partial t}+u\frac{\partial u}{\partial t}+v\frac{\partial u}{\partial t}+w\frac{\partial u}{\partial t}\right)=\rho F_x+\frac{\partial p}{\partial x}-\mu\left(\frac{\partial^2 u}{\partial x^2}+\frac{\partial^2 u}{\partial y^2}+\frac{\partial^2 u}{\partial z^2}\right), \tag{1.11}$$

$$\rho\left(\frac{\partial v}{\partial t}+u\frac{\partial v}{\partial t}+v\frac{\partial v}{\partial t}+w\frac{\partial v}{\partial t}\right)=\rho F_y+\frac{\partial p}{\partial x}-\mu\left(\frac{\partial^2 v}{\partial x^2}+\frac{\partial^2 v}{\partial y^2}+\frac{\partial^2 v}{\partial z^2}\right), \tag{1.12}$$

$$\rho\left(\frac{\partial w}{\partial t}+u\frac{\partial w}{\partial t}+v\frac{\partial w}{\partial t}+w\frac{\partial w}{\partial t}\right)=\rho F_z+\frac{\partial p}{\partial x}-\mu\left(\frac{\partial^2 w}{\partial x^2}+\frac{\partial^2 w}{\partial y^2}+\frac{\partial^2 w}{\partial z^2}\right). \tag{1.13}$$

1.6 Conservation of Energy

The conservation law of energy ensures that the total energy in a closed system remains unchanged. For this instance, we consider temperature (T) as the form of energy. So:

$$\rho\frac{\partial T}{\partial t}=k\nabla^2 T+\dot{q}+\phi_r. \tag{1.14}$$

where $\dot{q}$ is the rate of internal heat generation and ϕ_r is the viscous dissipation rate.

In the Cartesian coordinate system, this equation is:

$$\rho\left(\frac{\partial T}{\partial t}\right)+u\frac{\partial T}{\partial x}+v\frac{\partial T}{\partial y}+w\frac{\partial T}{\partial z}=k\left(\frac{\partial^2 T}{\partial x^2}+\frac{\partial^2 T}{\partial y^2}\right)+\dot{q}+\phi. \tag{1.15}$$

where ϕ_r is given by

$$\phi_r = 2\mu\left[\left(\frac{\partial u}{\partial x}\right)^2 + \left(\frac{\partial v}{\partial y}\right)^2 + \left(\frac{\partial w}{\partial z}\right)^2 + \frac{1}{2}\left(\frac{\partial v}{\partial x} + \frac{\partial u}{\partial y}\right)^2 + \frac{1}{2}\left(\frac{\partial w}{\partial y} + \frac{\partial v}{\partial z}\right)^2 + \frac{1}{2}\left(\frac{\partial u}{\partial z} + \frac{\partial w}{\partial x}\right)^2\right]. \tag{1.16}$$

1.7 Nanofluids

A nanofluid (NF) is a heat transfer fluid consisting of a base fluid (e.g., Propylene carbonate, oil, water, or ethylene glycol) and nanoparticles of size $10^{-9}m$. The nanoparticles typically consist of metal nitrides such as Aluminium Nitride (AlN) and Titanium Nitride (TiN), as well as oxide ceramics such as Zinc-Oxide (ZnO), Aluminium-Oxide (Al_2O_3), and Copper-Oxide (CuO), just to mention a few.

NFs have unique thermal, optical, and mechanical properties due to the presence of these nanoparticles. The primary characteristics of NFs are their improved thermal properties. Table 1.1. shows the thermophysical properties of NFs.

Table 1.1: Thermophysical properties of NFs

Quantity	Relation
Dynamic Viscosity	$\mu_{nf} = \mu_f(1-\phi)^{-2.5}$
Thermal Expansion	$(\rho\beta_T)_{nf} = (1-\phi)(\rho\beta_T)_f + \phi(\rho\beta_T)_s$
Heat Capacitance	$(\rho C_p)_{nf} = (1-\phi)(\rho C_p)_f + \phi(\rho C_p)_s$
Thermal Conductivity	$k_{nf} = k_f \frac{(k_s - 2\phi(k_f - k_s) + 2k_f)}{(k_s + 2\phi(k_f - k_s) + 2k_f)}$
Electrical Conductivity	$\frac{\sigma_{nf}}{\sigma_f} = 1 + \left\{3\left(\frac{\sigma_s}{\sigma_f} - 1\right)\phi\right\}\left\{\left(\frac{\sigma_s}{\sigma_f} + 1\right) - \left(\frac{\sigma_s}{\sigma_f} - 1\right)\phi\right\}^{-1}$

1.8 Hybrid Nanofluids

Hybrid nanofluids (HNFs) are heat transfer fluids that contain suspended nanoparticles of two or more different materials. In comparison to conventional nanofluids, HNFs are distinguished by their capacity to exhibit improved thermal conductivity, viscosity, and stability. The thermophysical properties of HNFs with two nanoparticles are shown in Table 1.2.

1.9 Prandtl Number

The Prandtl number quantifies the relationship between the diffusion of momentum and the diffusion of heat in a fluid, expressed as a dimensionless quantity. It is typically denoted Pr. It

Table 1.2: Thermophysical properties of HNFs

Quantity	Relation
Dynamic Viscosity	$\mu_{hnf} = \mu_f(1-\phi_1)^{-2.5}(1-\phi_2)^{-2.5}$
Thermal Expansion	$(\rho\beta_p)_{hnf} = (1-\phi_2)[(1-\phi_1)\rho\beta_p)_f + \phi_1(\rho\beta_p)_{n1}] + \phi_2(\rho\beta_p)_{n2}$
Heat Capacitance	$(\rho C_p)_{hnf} = (1-\phi_2)[(1-\phi_1)\rho C_p)_f + \phi_1(\rho C_p)_{n1}] + \phi_2(\rho C_p)_{n2}$
Thermal Conductivity	$\frac{k_{hnf}}{k_f} = \frac{k_{n2}+(m-1)k_{bf}-(m-1)\phi_2(k_{bf}-k_{n2})}{k_{n2}+(m-1)k_{bf}+\phi_2(k_{bf}-k_{n2})}$
Electrical Conductivity	$\frac{\sigma_{hnf}}{\sigma_f} = 1 + \frac{3\phi\left(\phi_1\sigma_1+\phi_2\sigma_2-\sigma_{bf}(\phi_1+\phi_2)\right)}{\phi_1\sigma_1+\phi_2\sigma_2+2\phi\sigma_{bf}-\phi\sigma_{bf}\left(\phi_1\sigma_1+\phi_2\sigma_2-\sigma_{bf}(\phi_1+\phi_2)\right)}$, $\phi = \phi_1+\phi_2$

is represented mathematically as:

$$Pr = \frac{\nu}{\alpha} = \frac{\frac{\mu}{\rho}}{\frac{\kappa}{(\rho C_p)}} = \frac{(\rho C_p)}{\kappa}. \tag{1.17}$$

1.10 Grashof Number

The Grashof number, denoted Gr, is a dimensionless number that describes the relationship between buoyancy and viscosity in a fluid flow system. It is formulated as:

$$Gr = \frac{g(\rho B_t)_f(T_W - T_\infty)}{\nu^3}. \tag{1.18}$$

1.11 Nusselt Number

In heat transfer analysis, the Nusselt number is a dimensionless quantity that characterizes the ratio of convective to conductive heat transfer across a fluid boundary. Mathematically denoted as Nu, it is represented as:

$$Nu_x = \frac{xq_w}{k_f(T_W - T_\infty)}. \tag{1.19}$$

1.12 Skin friction coefficient

The skin friction coefficient is a dimensionless parameter that quantifies the reduction of fluid motion due to the presence of friction, typically denoted by C_f. It is represented mathematically as:

$$C_f = \frac{\tau_w}{\rho_f U_w^2}. \tag{1.20}$$

1.13 Radiation

Radiation takes place through the emission of photons or waves from a surface or a volume of space, and it can occur even in a vacuum, and at any temperature above absolute zero. The Stefan-Boltzmann law is utilized for the computation of the quantity of energy that is transmitted via radiation. Mathematically, it is represented as:

$$q = \sigma^* \cdot T^4. \tag{1.21}$$

1.14 Casson Fluid

According to the definition proposed by Casson in his research on flow properties, the Casson fluid is a type of shear thinning liquid that demonstrates an infinitely high viscosity at zero shear rate [4]. Although the Casson fluid model has its origins as modelling the flow of paints, gels, and creams, it acts as an ideal model for various engineering disciplines and biological applications. For example, biomedical engineering the Casson fluid model has been used for modelling the flow of blood in narrow arteries. The Casson fluid has been studied extensively in different heat conditions, surface conditions and various boundary conditions. An ideal model for a particular situation is normally developed from the use of suitable initial conditions to solve the governing equations.

Casson fluid shear stress can be described using the equation:

$$\tau_{ij} = \begin{cases} 2\left(\mu_B + \frac{p_r}{\sqrt{2\pi_c}}\right) e_{ij}, & \text{if } \pi < \pi_c \\ \\ 2\left(\mu_B + \frac{p_r}{\sqrt{2\pi}}\right) e_{ij}, & \text{if } \pi > \pi_c, \end{cases} \tag{1.22}$$

where p_r, μ_B, π_c denote the yield stress, plastic dynamic viscosity, and product of μ_B and p_r respectively, and $\pi = e_{ij}e_{ij}$.

1.15 Fractional Order Derivatives

Fractional calculus is a mathematical discipline that generalizes the concepts of differentiation and integration to non-integer orders. Numerous disciplines use fractional calculus, including physics, engineering, finance, biology, control systems, and many more.

There are different definitions of fractional derivatives, each with its own mathematical formulation and properties. Some of the commonly used definitions of fractional derivatives are discussed below.

1.15.1 Caputo fractional derivative

This definition was proposed by Michele Caputo in 1967 [5]. Mathematically, it is represented as follows:

$$ {}^{C}D_t^{\alpha} f(\tau) = \frac{1}{\Gamma(\alpha - n)} \int_a^t \frac{f^{(n)}(\tau)}{(t-\tau)^{\alpha+1-n}} f'(\tau) d\tau. \tag{1.23} $$

1.15.2 Caputo - Fabrizio fractional derivative

This method was developed in 2015 by Michele Caputo and Mauro Fabrizio[6]. It is defined:

$$ {}^{CF}D_t^{\alpha} f(\tau) = \frac{1}{1-\alpha} \int_0^t exp\left(\frac{-\alpha(t-\tau)}{1-\alpha}\right) f'(\tau) d\tau. \tag{1.24} $$

1.15.3 Atangana - Baleanu fractional derivative (ABFD)

This method was suggested by Abdon Atangana and Dumitru Baleanu in 2016[7]:

$$ {}^{AB}D_t^{\alpha} f(\tau) = \frac{1}{1-\alpha} \int_0^t E_{\alpha}\left(\frac{-\alpha(t-\tau)}{1-\alpha}\right) f'(\tau) d\tau, \tag{1.25} $$

where

$$ E_{\alpha}(-t^{\alpha}) = \sum_{k=0}^{\infty} \frac{(-t)^{\alpha k}}{\Gamma(\alpha k + 1)}. \tag{1.26} $$

is the Mittag-Leffer function.

1.15.4 Prabhakar fractional derivative (PBFD)

This method finds its roots in the work of Tilak Raj Prabhakar, an Indian mathematician [8]. By making use of the Mittag-Leffer function with three parameters, known as the Prabhakar function, the implementation of fractional calculus is achieved. The PBFD can be mathematically defined as:

$$ \begin{aligned} {}^{PB}\mathfrak{D}^{\gamma}_{\alpha,\beta,\gamma} g(t) &= E^{-\gamma}_{\alpha,k,-\beta,\alpha} g(t) \\ &= e^{-\gamma}_{\alpha,k,-\beta}(\alpha; t) * g^k(t) \\ &= \int_0^t (t-\tau)^{k-\beta-1} E^{-\gamma}_{\alpha,k,-\beta,\alpha}(\alpha(t-\tau)^{\alpha}) g^k(\tau) d\tau. \end{aligned} $$

The notation g^k signifies the k^{th} derivative of $g(t) \in AC^k(0,b)$, where $AC^k(0,b)$ represents a real-valued function with continuous derivatives of order $(k-1)$ within the interval $(0,b)$. The Prabhakar integral is identified as:

$$E^{-\gamma}_{\alpha,k,\alpha}g(t) = \int_0^t (t-\tau)^{k-\beta-1} E^{-\gamma}_{\alpha,k,-\beta,\alpha}(\alpha(t-\tau)^{\alpha}) g^k(\tau) d\tau,$$

and

$$E^{-\gamma}_{\alpha,\beta}(z) = \sum_{p=0}^{\infty} \frac{\Gamma(\gamma+p)z^p}{p!\Gamma(\gamma)\Gamma(\alpha p+\beta)},$$

represents the three-parameter Mittag-Leffer function.

Fractional order derivatives have been successfully applied in many fields including physics, electrochemistry,bio-engineering, signal processing, fluid mechanics and microbiology [9]. Fractional differential equations are differential equations which involve fractional derivatives. These differential equations can typically be solved using the Laplace transform method. The procedure is in this manner: Derive the governing equations and corresponding IC and BC for the problem, find the Laplace transformation of the equations, solve for the unknown function's transform, and finally find the inverse Laplace transform (analytically or numerically) to get the required result. This is the method that we will employ in this thesis.

1.16 Objectives

The present study seeks to use two different definitions of fractional derivatives to study the dynamics of Casson NF and HNF. The primary goals of this thesis are outlined as follows.

- To derive and solve the governing equations for the blood NF (with MWCNTs and SWCNTs) and blood HNF (Copper and Aluminium Oxide) flowing over a vertical plate with applied thermal radiation, vibration condition, and oscillating plate using the Casson fluid model.
- To use the PBFD and ABFD, respectively, to study the dynamics of the problems.
- To evaluate the effectiveness of these fractional order derivatives in modeling the behavior of blood NF and HNF.
- To investigate how the velocity and temperature distributions of NFs and HNFs are influenced by various parameters, such as fractional orders, nanoparticle volume fraction, Prandtl number, Grashof number, Nusselt number, Skin friction, applied radiation and vibration.

1.17 Thesis Outline

- Chapter 1 provides an introduction to fluid flow and the fundamental principles of conservation laws, along with a concise overview of NFs and HNFs. The Casson fluid model and key dimensionless fluid dynamics parameters are discussed, as well as the thesis objectives.

- Chapter 2 presents a literature review summarizing the topics of NFs, effects of vibration on the body, oscillating flow, nanoparticles, nanoparticle shape effects, and fractional order calculus and its applications in fluid dynamics.
- Chapter 3 seeks to apply the PBFD to study the flow of SWCNT/Casson and MWCNT/-Casson NFs flowing over a vertical plate with radiation and vibration condition.
- The investigation in Chapter 4 involves the implementation of the Atangana-Baleanu fractional definition to analyze the flow properties of a $Cu - Al_2O_3$/Casson HNF subjected to an oscillating surface with thermal radiation, with special consideration given to the effects of nanoparticle shape.
- Finally, Chapter 5 outlines the conclusions drawn from the present research and discusses future directions.

2. Literature Review

Nanotechnology is the science and discipline of the creation and use of nanometer sized particles called nanoparticles. In recent years, research in nanotechnology has exploded as a result of the vast range of its applications. Nanotechnology has improved our quality of life in many different aspects. For instance nanotechnology has been applied successfully in manufacturing, biology, industry and electronics. It has also been used in medicine and medical procedures in making them safer, cheaper and easier to administer [10].

Nanofluids (NFs) are a key component of nanotechnology. NFs are a class of fluids that contain suspended nanometer-sized ($10^{-9}m$) particles, such as metal or oxide nanoparticles[11]. They are obtained by dispersing nanoparticles in a typical base fluid such as Ethylene glycol, Propylene carbonate, different types of oils, and water, to form a stable suspension. The pioneering work of Choi et al. [12] introduced the term "nanofluid" and provided an initial understanding of its properties. Nanoparticles are typically metals such as Copper (Cu), Silver (Ag), oxide ceramics such as Aluminium Oxide (Al_2O_3), Titanium Oxide (TiO), and nitride metals like Titanium Nitride (TiN) and Aluminium Nitride (AlN), just to name a few [13]. The objective of creating a NF is to improve the thermal characteristics of a regular base fluid. As a result, NFs have unique physical properties of viscosity, specific heat, thermal conductivity and stability. The ability to have better control of the thermal properties of NFs over typical base fluids has led to NFs being a highly researched area. Furthermore, the unique characteristics of NFs make them potentially helpful in a wide range of applications. NFs have been used successfully in fields such as nanotechnology, bio-medical, automotive, manufacturing, plasma physics and more [14]. In particular, the thermal properties of NFs are a popular research interest lately. The reason for investigating NFs is mainly due to their superior thermal properties. As a result, several authors have studied NFs and their applications in the fluid mechanics domain. Shaw et al. [15] examined the impact of slip conditions on the nonlinear convection behavior of NF flow over stretching sheets. Kumar et al. [16] analyzed the flow of an unsteady micro-polar NF flow though a squeezing channel with activation energy with applications in drug delivery. Saeed et al. [17] investigated the flow of blood based HNF with electromagnetic field condition and coupled stresses. In their investigation, Sahu et al. [18] analyzed the thermal management of SWCNT–MWCNT Cross HNF flow resulting from a vertically stretched cylinder, considering situations with and without inertia effects. Noreen et al. [19] analyzed the blood flow considering the NF effects in a vertical channel. In their research, Shah et al. [20] examined the behavior of micro-polar gold-blood NF flow in permeable channels, taking into account the influence of radiative heat transfer.

Hybrid nanofluids (HNFs), on the other hand, are a recent development that combines the advantages of two or more types of nanoparticles or base fluids to achieve superior thermal properties. HNFs include typical base fluids with a combination of nanoparticles such as Multi-

walled carbon nanotubes and copper oxide (MWCNT - CuO) [21], Graphene oxide and boron nitride (GO - BN) [22], Titanium dioxide and carbon nanotubes (TiO_2 - CNTs)[23] and Aluminium Zinc (Al - Zn) HNFs [24], just to name a few. HNFs are finding increasing applications in various industrial processes, including cooling of electronic devices, heat exchangers, and solar collectors [25]. As a result, the development and use of HNFs have also become an active area of research in the field of nanotechnology and material science. In the field of fluid mechanics, several authors have studied HNFs extensively. The magnetic flow of nanomaterials between two parallel, permeable and stretching/shrinking surfaces was compared by Nayak et al. [26]. In their research, Shaw et al. [27] investigated the effect of entropy generation and nonlinear thermal radiation on the Darcy-Forchheimer flow dynamics of $MnFe_2O_4$-Casson/water NF induced by rotating disks.

In the field of fluid dynamics, fluids are commonly classified as either Newtonian or non-Newtonian fluids. Blood is a non-Newtonian fluid that exhibits shear-thinning behavior, which means that its viscosity decreases as the shear rate increases. To model the rheological behavior of blood, several mathematical models have been proposed, including the Casson fluid model [4]. The Casson model assumes that blood consists of a suspension of non-deformable particles in a fluid that behaves like a viscous liquid. This model has been used to study blood flow in the human body and understand the mechanisms behind several cardiovascular diseases. The main function of blood is to transport nutrients and oxygen to various parts of the body. The thermal behavior of blood is governed by its components, which include platelets, plasma, red blood cells and white blood cells. The concentration and size of these components are key factors. As a result of this, blood exhibits some unique thermal characteristics. As such, several authors have studies the thermal effects of blood as a base fluid. In their work, Alghamdi et al. [28] investigated the flow behavior of a Casson HNF with copper aluminium nanoparticles as it reached a stagnation point on a stretching surface. Saeed et al. [29] investigated the flow of HNFs with blood as the base fluid, with couple stresses by the convergent as well as divergent channel, with applications in drug delivery . They also investigated blood based HNF flow while considering electromagnetic field and couple stresses, with carbon nanotubes as the nanoparticles [17].

Under whole-body vibration, the circulatory system's blood flow is greatly disrupted. Instances where such a situation can occur include flying in an aircraft, travelling in a vehicle on a bumpy road, and working in any vibrating environment. Severe vibrating environments greatly affect peripheral blood flow and muscle oxygenation [30]. Observed effects of being in a vibrating environment include as fatigue, elevated blood pressure, headaches, vision loss and stomach problems. In severe cases, vibration can damage the red blood cells and platelets, which can lead to blood clogging. As a result, several studies have been made on the vibrational effect of blood flow, in both normal and diseased pathological states. Maiti et al. [31] examined the thermochemical flow of blood with magnetic and vibration environment, taking into account the Dufour and Soret effects. Kadhim et al. [32] observed how induced vibration affects blood flow properties in a mechanical aortic valve.

A well-known cause of increased mass and heat transmission is oscillating flow. Oscillating flow has proven to be useful as compared to non-oscillating flow. As a result, oscillating flow has been used and applied in a massive range of medical and engineering domains [33]. Thus, many authors have studied the effects of oscillating flow on different fluids with different conditions. For instance, the research conducted by Ali et al. [34] examined the solutions of unsteady free convection in a closed arrangement for the flow of second-grade fluids on a perpendicular plate with oscillations. Shah et al. [35] used time-fractional Caputo-Fabrizio derivatives to observe thermal analysis of second-grade fluids over an oscillation perpendicular flat plate. The MHD free convective flow of Casson fluid through a porous medium, induced by a vertically oscillating plate, was studied using the finite difference method in a recent study conducted by Goud et al. [36]. Abdel-Gawad [37] did a stability analysis of steady and unsteady flows as well as heat transfer in Casson fluid over a free stretching, oscillating surface.

Carbon nanotubes (CNTs) are formed by rolling graphite sheets into cylindrical shapes [38] which possess incredible thermal properties. CNTs have a vast range of applications in many different fields including electronics and microelectronics, optics, medicine, energy storage and others [39]. They are particularly useful in medicine, for example for drug delivery and biosensing equipment [40]. CNTs are classified into two main types being single-walled carbon nanotubes (SWCNTs) and multi-walled carbon nanotubes (MWCNTs). Researchers have investigated the flow behavior of CNT NFs in various contexts. Gul et al. [41] observed the flow of NF over carbon nanotubes in the region between a disk and a cone in a spinning system. The study by Wang et al. [42] focused on examining the flow characteristics of blood-based carbon nanotubes under Newtonian heating conditions using the PBFD.

Aluminium oxide (Al_2O_3) and Copper (Cu) have been a popular choice for nanoparticles in HNFs, mainly due to the excellent thermal properties of the individual nanoparticles. The performance of these nanoparticles has been assessed in various settings by multiple researchers. Moghadassi et al. performed a numerical investigation to analyze the influence of water-based aluminium and aluminium-copper HNFs on forced convective heat transfer. Using the Caputo fractional derivative, Ahmed [43] analyzed the convective flow in an inclined wavy vented cavity filled with a porous medium containing $Al_2O_3 - Cu$ hybrid nanofluids. In a study by Ijaz [44], the impact of wall characteristics on the shape factor and sphericity features of copper and $Cu - Al_2O_3$ with blood in an atherosclerotic artery was investigated. On the other hand, Alghamadi et al. [45] did an study on the magnetohydrodynamic flow of HNF comprising of medication through a blood artery. Yasir et al. [46] performed a comparative analysis of hybrid Cu-Al_2O_3 nanomaterials on the flow characteristics over a stretching/shrinking cylinder with radiative effects. The work of these authors generally indicate that $Al_2O_3 - Cu$ HNFs have superior thermal properties as compared to many types of NFs.

In fractional calculus, the derivative and integral operations are extended to non-integer orders, providing a more comprehensive framework for modeling intricate real-world phenomena. As a result, it has been successfully applied across many fields such as fluid mechanics, physics,

biomathematics, finance, signal processing and electrochemistry. The most popular fractional calculus techniques are Caputo [5], Caputo-Fabrizio [6] and Atangana-Baleanu types. As such, Yavuz and Özdemir [47] did a comparison between Caputo-Fabrizio and Atangana-Baleanu fractional (ABFD) operators with exponential and Mittag-Leffer kernel [47]. Their results indicated a good stability for both methods when using the Laplace homotopy transformation method. A very essential function in fractional calculus is the Mittag-Leffer function. In 1971, Prabhakar introduced a three-parameter Mittag-Leffer function, commonly referred to as the Prabhakar function [8]. Garra and Garrapa [48] studied the theory and applications of the Prabhakar function extensively. The Prabhakar fractional derivative (PBFD) has been used successfully by various researchers in fluid mechanics. The convective behavior of Casson fluid across an oscillating surface was explored by Sarwar et al. [49] using PBFD simulations, with consideration for the generalized Fourier law. The research conducted by Wang et al. [50] involved studying the unsteady thermal transport flow of Casson NFs using the generalized Mittag–Leffer kernel of Prabhakar's type. The study by Jie et al. [51] focused on studying the thermal flow of Brinkman type NF containing carbon nanotubes by utilizing PBFD simulations under sinusoidal oscillations. The ABFD is a relatively new type of fractional derivative that has been introduced in recent years. It contains two parameters that control the order of the derivative and the degree of the memory effect. It has also been used to study various fluid mechanics problems, including flow through porous media and biofluids. The behavior and properties of SWCNTs and MWCNTs nanoparticles in blood with ramped temperature were studied by Raza et al. [52] using the ABFD.

The shape of nanoparticles has been shown to have a significant effect on the temperature and velocity profiles of HNFs. In general, nanoparticles with more elongated or anisotropic shapes, such as nanorods or nanowires, have been found to enhance thermal conductivity and heat transfer in NFs more effectively than spherical nanoparticles due to their increased surface area and enhanced interfacial interactions. However, the exact effects of nanoparticle shape on NF properties can depend on a variety of factors, including the material composition of the nanoparticles and the base fluid, as well as the concentration and size of the nanoparticles. As a result, several authors have studied the effects of the shape of nanoparticles. Timofeeva et al. [53] studied the effects of shape of particles on the thermophysical properties of alumina NFs. Tripathi et al. [54] investigated the dynamics of nanoparticle shape on Copper and copper oxide/blood flow in an electromagnetic field.

Based on the literature reviewed, it appears that no prior research has employed the PBFD to investigate the behavior of thermal Casson NF flow in the presence of SWCNT and MWCNT, subject to radiation and vibration conditions. Similarly, the utilization of the ABFD for the study of Copper-Aluminium Oxide/Casson HNF flow over a vertical oscillating plate, with radiation effects, taking into account the influence of particle shape, has not been explored in the literature. The present study aims to address this research gap by employing these fractional derivatives to investigate the aforementioned flow problems.

3. Prabhakar fractional simulation of thermal Casson nanofluid flow with SWCNT and MWCNT in radiation and vibrating conditions

3.1 Introduction

Using numerical techniques, this chapter investigates the flow and heat transfer behavior of blood NF. The results are graphically presented, allowing for a comprehensive understanding of the effects of different parameters on the temperature and velocity distributions. The Casson fluid model is employed to simulate blood. The ILT will be computed numerically using Tzou [55] and Zakian [56] schemes.

In view of the aforementioned literature and related articles (see Chapter 2), this chapter aims:

- To use fractional calculus to investigate the thermal and velocity outcomes of blood based NF flowing within a magnetic field in carbon nanotubes with radiative heat flux and a vibrating environment.
- To adopt the Casson fluid model to investigate the shear thickening and shear thinning properties of blood as a base fluid.
- To utilize the PBFD technique and the Laplace transformation method to carry out the fractional simulations.
- To find the solutions by simulating the inverse of the Laplace numerically using Tzuo's method and Zakian's method, and analyse the physical interpretations of the results.

3.2 Mathematical Model

We consider the free convective flow of blood-nanoparticle over a permeable vertical plate with radiative flux and vibration. Blood is considered as Casson fluid. A magnetic field of strength B_0 is applied at an angle θ. The temperature at the surface is represented by T_W, while the ambient temperature is denoted as T_∞. The nanoparticles of interest are Single-wall carbon nanotubes and multi-wall carbon nanotubes (SWCNTs and MWCNTs). The thermophysical properties of the base fluid and nanoparticles are shown in Table (3.1). Initially, the fluid is at rest and at ambient temperature. The velocity profile of the fluid is characterized by a power-law dependence on time at the boundary, with the exponent p dictating the specific behavior of the profile. This indicates the sudden motion of a boundary. It is also assumed that the applied radiation is not affected by velocity. Figure 3.1 shows the geometry of the problem to be studied.

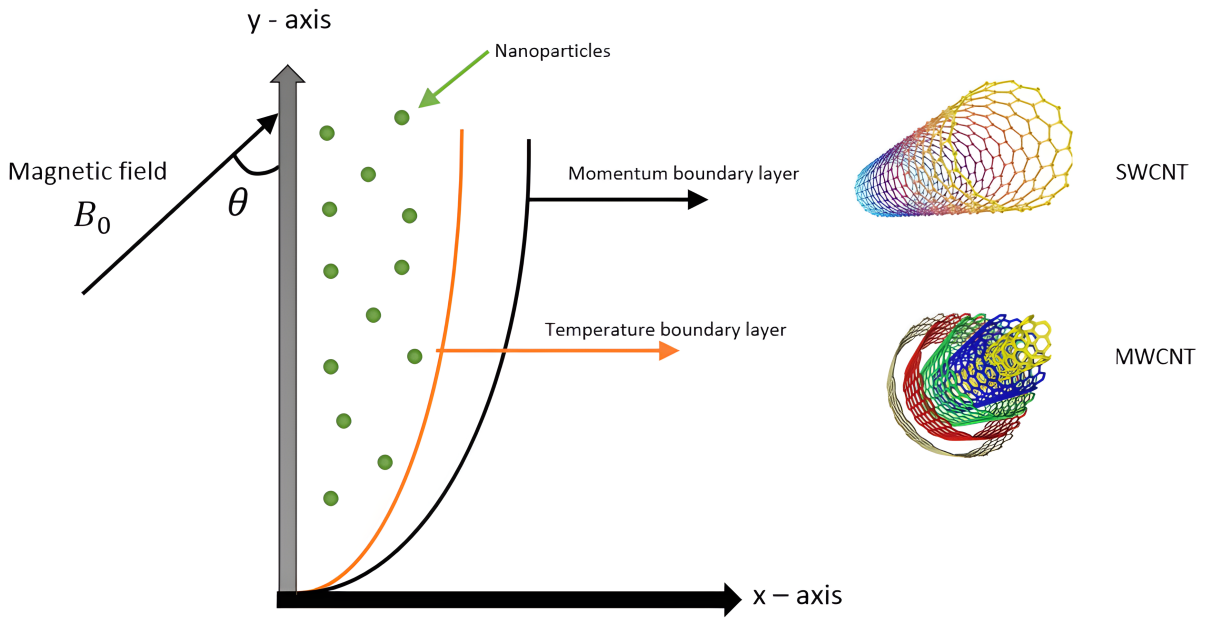


Figure 3.1: Geometry of flow

Table 3.1: Thermophysical properties of blood and carbon nanotubes

Material	Blood	SWCNT	MWCNT
ρ (kg/m^3)	1053	2600	1600
C_p (J/kgK)	3594	425	796
σ	0.8	$10^6 - 10^7$	1.9 $\times 10^{-4}$
k (W/mK)	0.492	6600	3000
β_T $\times 10^{-5}(K^{-1})$	0.18	27	44

As noted in equation (1.22), the rheological properties of Casson fluid [4] are given as:

$$\tau_{ij} = \begin{cases} 2\left(\mu_B + \frac{p_r}{\sqrt{2\pi_c}}\right) e_{ij}, & \text{if } \pi < \pi_c, \\ 2\left(\mu_B + \frac{p_r}{\sqrt{2\pi}}\right) e_{ij}, & \text{if } \pi > \pi_c, \end{cases} \tag{3.1}$$

where the variables p_r, μ_B, and π_c represent the yield stress, plastic dynamic viscosity, and the product of μ_B and p_r respectively.

The governing equations for the system, assuming the above conditions, can be formulated as:

- Momentum Equation

$$\rho_{nf}\frac{\partial v^*}{\partial t^*} = \mu_{nf}\left(1 + \frac{1}{\beta_0}\right)\frac{\partial^2 v^*}{\partial \xi^{*2}} - \left(\sigma_{nf}B_0^2 sin\theta + \frac{\mu_{nf}}{\kappa}\right)v^* + g(\rho B_T)_{nf}(T^* - T_\infty) + K_0 Cos(\kappa_0 t^* + \phi_0), \tag{3.2}$$

Table 3.2: Thermophysical properties of NFs

Quantity	Relation
Dynamic Viscosity	$\mu_{nf} = \mu_f(1-\phi)^{-2.5}$
Thermal Expansion	$(\rho\beta_T)_{nf} = (1-\phi)(\rho\beta_T)_f + \phi(\rho\beta_T)_s$
Heat Capacitance	$(\rho C_p)_{nf} = (1-\phi)(\rho C_p)_f + \phi(\rho C_p)_s$
Thermal Conductivity	$k_{nf} = k_f \frac{(k_s - 2\phi(k_f-k_s)+2k_f)}{(k_s+2\phi(k_f-k_s)+2k_f)}$
Electrical Conductivity	$\frac{\sigma_{nf}}{\sigma_f} = 1 + \left\{3\left(\frac{\sigma_s}{\sigma_f}-1\right)\phi\right\}\left\{\left(\frac{\sigma_s}{\sigma_f}+1\right) - \left(\frac{\sigma_s}{\sigma_f}-1\right)\phi\right\}^{-1}$

- Energy Equation

$$(\rho C_p)_{nf}\frac{\partial T^*(\xi^*,t^*)}{\partial t^*} = -\frac{\partial q^*(\xi^*,t^*)}{\partial \xi^*}, \tag{3.3}$$

- Radiative Heat Flux under Rosseland approximation [57]

$$q^* = -\frac{4\sigma^*}{3k^*}\frac{\partial}{\partial \xi^*}T^{*4}_{(\xi^*,t^*)}. \tag{3.4}$$

Employing the Taylor series expansion of T^{*4} about T_∞ and neglecting the second- and higher-order contributions in $(T^* - T_\infty)$ (because they will have negligible influence on the overall behavior of the expression), we arrive at the following expression:

$$T^{*4} \approx 4T_\infty^3 T^* - 3T_\infty^4. \tag{3.5}$$

The specified IC and BC are given by:

$$\begin{aligned} &v^*(\xi^*,0) = 0, && T^*(\xi^*,0) = T_\infty, \quad \forall \xi^* \geq 0, \\ &v^*(0,t^*) = v_0 t^{*p}, && \left.\frac{\partial T^*(\xi^*,t^*)}{\partial \xi^*}\right|_{\xi^*=0} = \frac{h}{k}T^*(\xi^*,t^*), \quad t^* > 0, p > 0 \\ &v^*(\xi^*,t^*) \to 0, && T^*(\xi^*,t^*) \to 0, \quad \xi^* \to \infty, t^* > 0. \end{aligned} \tag{3.6}$$

To non-dimensionalise the above system, we introduce the following dimensionless variables:

$$\begin{aligned} v^* &= \frac{v}{v_0}, & q^* &= \frac{q}{q_0}, & t^* &= \frac{v_0^2}{v_f}t, \\ T^* &= \frac{T(\xi,t)-T_\infty}{T_W - T_\infty}, & \xi^* &= \frac{v_0}{v_f}\xi, & q_0 &= k_f\frac{(T_W - T_\infty)v_0}{v_f}. \end{aligned} \tag{3.7}$$

Using (3.5) and (3.4) in (3.3), and using the above dimensionless variables, and dropping the * sign, the equations eqs. (3.2) to (3.4) simplify to:

$$\eta_0 \frac{\partial v(\xi,t)}{\partial t} = \frac{\eta_1}{\beta_1}\frac{\partial^2 v(\xi,t)}{\partial \xi^2} - \left(\eta_2 MSin\theta + \frac{\eta_1}{\kappa}\right) + \eta_3 GrT(\xi,t) + HCos(\kappa_0 t + \phi_0), \tag{3.8}$$

$$\eta_4 Pr \frac{\partial T(\xi,t)}{\partial t} = -\eta_5 \frac{\partial q(\xi,t)}{\partial \xi}, \tag{3.9}$$

$$q(\xi,t) = -R\frac{\partial T(\xi,t)}{\partial \xi}, \tag{3.10}$$

with conditions

$$\begin{aligned} &v(\xi,0) = 0, && T(\xi,0) = 0, \quad \forall \xi \geq 0, \\ &v(0,t) = t^p, && \left.\frac{\partial T(\xi,t)}{\partial \xi}\right|_{\xi=0} = -(1 + T_{(0,t)}), \quad t > 0, p > 0, \\ &v(\xi,t) \to 0, && T(\xi,t) \to 0, \quad \xi \to \infty, t > 0, \end{aligned} \tag{3.11}$$

where

$$M = \frac{v_f \sigma_f B_0^2}{\rho_f v_o^2}, \qquad R = -\frac{16\sigma^* T_\infty^3}{3k^*}, \qquad \beta_1 = \frac{\beta_0}{1+\beta_0},$$
$$Pr = \left(\frac{\mu C_p}{\kappa}\right)_f, \qquad k = \frac{\kappa v_o^2}{v_f \phi}, \qquad Gr = \frac{g(\rho B_t)_f (T_W - T_\infty)}{\nu^3},$$

represent the Magenetic parameter (M), Radiation number (R), Casson fluid parameter (β_1) , Prandtl Number (P_r), permeability constant (k), Grashof number (Gr). The constants related to volume fraction of the nanoparticles are $\eta_0, \eta_1, \eta_2, \eta_3, \eta_4$, and η_5 , and they are defined as:

$$\eta_0 = (1-\phi) + \phi\frac{\rho_s}{\rho_f}, \qquad \eta_1 = \frac{1}{(1-\phi)^{2.5}},$$
$$\eta_3 = (1-\phi) + \phi\frac{(\rho B_T)_s}{\rho B_T)_f}, \quad \eta_4 = (1-\phi) + \phi\frac{(\rho C_T)_s}{\rho C_T)_f}, \quad \eta_5 = \frac{(1-\phi) + 2\phi\frac{k_s}{k_s-k_f} ln\left(\frac{k_s-k_f}{2k_f}\right)}{(1-\phi) + 2\phi\frac{k_s}{k_s-k_f} ln\left(\frac{k_s+k_f}{2k_f}\right)},$$

$$\eta_2 = 1 + \left\{3\left(\frac{\sigma_s}{\sigma_f} - 1\right)\phi\right\}\left\{\left(\frac{\sigma_s}{\sigma_f} + 1\right) - \left(\frac{\sigma_s}{\sigma_f} - 1\right)\phi\right\}^{-1}.$$

3.3 Prabhakar Fractional Order

The PBFD is implemented

$$q(\xi,t) = -{}^{PB}\mathfrak{D}^{\gamma}_{\alpha,\beta,\gamma} R\frac{\partial T}{\partial \xi}, \tag{3.12}$$

where ${}^{PB}\mathfrak{D}^{\gamma}_{\alpha,\beta,\gamma}$ symbolizes the regularised PBFD [48], which is defined:

$$\begin{aligned} {}^{PB}\mathfrak{D}^{\gamma}_{\alpha,\beta,\gamma} g(t) &= E^{-\gamma}_{\alpha,k,-\beta,\alpha} g(t) \\ &= e^{-\gamma}_{\alpha,k,-\beta}(\alpha;t) * g^{(k)}(t) \\ &= \int_0^t (t-\tau)^{k-\beta-1} E^{-\gamma}_{\alpha,k,-\beta,\alpha}(\alpha(t-\tau)^{\alpha}) g^{(k)}(\tau). \end{aligned}$$

In this context, $g^{(k)}$ represents the k^{th} derivative of $g(t) \in AC^k(0,b)$, with $AC^k(0,b)$ denoting a real-valued function having continuous derivatives of $(k-1)$ order within the interval $(0,b)$. The Prabhakar integral is identified as:

$$E^{-\gamma}_{\alpha,k,\alpha} g(t) = \int_0^t (t-\tau)^{k-\beta-1} E^{-\gamma}_{\alpha,k,-\beta,\alpha}(\alpha(t-\tau)^{\alpha}) g^{k}(\tau) d\tau,$$

and

$$E^{-\gamma}_{\alpha,\beta}(z) = \sum_{p=0}^{\infty} \frac{\Gamma(\gamma+p) z^p}{p! \cdot \Gamma(\gamma) \cdot \Gamma(\alpha m+\beta)},$$

represents the three-parameter Mittag-Leffer function. The Laplace of the Prabhakar operator ${}^{PB}\mathfrak{D}^{\gamma}_{\alpha,\beta,\gamma}$ is implemented as:

$$\begin{aligned} \mathcal{L}[{}^{PB}\mathfrak{D}^{\gamma}_{\alpha,\beta,\gamma}] &= \mathcal{L}[h^m(t) * e^{-\gamma}_{\alpha,k,-\beta}(\alpha;t)] \\ &= \mathcal{L}[h^m(t)] \cdot \mathcal{L}[e^{-\gamma}_{\alpha,k,-\beta}(\alpha;t)] \\ &= \mathcal{L}[h^m(t)] s^{\beta-m}(1-\alpha s^{-\alpha})^{\gamma}, \end{aligned} \tag{3.13}$$

where the Fourier's law is obtained when $\gamma = \beta = 0$.

3.4 Solution of the problem

3.4.1 Solution of the temperature profile [Equations (3.9) and (3.12)]

Here we suppose that $\beta \in [0,1)$, and take $m = 0$ in (3.13). By taking the Laplace transformations of equations (3.9) and (3.12) and on its accompanying conditions, we get:

$$\eta_4 Prs\overline{T}(\xi,t) = -\eta_5 \frac{\partial \overline{q}(\xi,t)}{\partial \xi}, \tag{3.14}$$

$$\overline{q} = s^{\beta}(1-\alpha s^{-\alpha})^{\gamma} R \frac{\partial \overline{T}(\xi,t)}{\partial \xi}, \tag{3.15}$$

with the initial condition

$$\frac{\partial \overline{T}}{\partial \xi} = -\left(\frac{1}{s} + \overline{T}_{(0,s)}\right). \tag{3.16}$$

Using (3.15) in (3.14) we obtain the differential equation

$$\frac{\partial^2 \overline{T}(\xi,t)}{\partial \xi^2} - \frac{\eta_4 Pr}{\eta_5 R} \frac{s^{1-\beta}}{(1-\alpha s^{-\alpha})^{\gamma}} \overline{T} = 0. \tag{3.17}$$

Applying the initial conditions (3.11) and (3.16), we obtain the solution to (3.17) as

$$\overline{T}_{(\xi,s)} = \frac{1}{s\left(\sqrt{\frac{\eta_4 Pr}{\eta_5 R}\frac{s^{1-\beta}}{(1-\alpha s^{-\alpha})^{\gamma}}}\right)} e^{-\xi\sqrt{\frac{\eta_4 Pr}{\eta_5 R}\frac{s^{1-\beta}}{(1-\alpha s^{-\alpha})^{\gamma}}}}, \tag{3.18}$$

where $\overline{T}$ is the solution of the temperature profile in the s-domain (Laplace domain).

3.4.2 Solution of the velocity profile [Equation (3.8)]

By employing Laplace transformations on (3.8) and considering its accompanying IC and BC, we arrive at the resulting non-homogeneous differential equation.

$$\eta_0 s\overline{v}_{(\xi,s)} = \frac{\eta_1}{\beta_1}\frac{\partial^2 \overline{v}_{(\xi,s)}}{\partial \xi^2} - \left(\eta_2 M sin\theta + \frac{\eta_3}{k}\right)\overline{v}_{(\xi,s)} + \eta_3 Gr\overline{T}_{(\xi,s)} + H\left[\frac{scos\phi_0 + \kappa_0 sin\phi_0}{s^2+\kappa_0^2}\right], \tag{3.19}$$

$$\overline{v}_{(0,s)} = \frac{p!}{s^{p+1}}; \quad \overline{v}_{(\xi,s)} \to 0 \text{ as } \xi \to \infty.$$

Solving (3.19) using it's accompanying initial conditions, we obtain solution in the s-domain as:

$$\overline{v}_{(\xi,s)} = \left(\frac{p!}{s^{p+1}} - \frac{C}{B} - \frac{D}{L-B}\right)e^{-\xi\sqrt{B}} + \left(\frac{C}{B} + \frac{D}{L-B}\right)e^{-\xi\sqrt{L}}, \tag{3.20}$$

with the constants B, C, D, and L defined in the Appendix A.

The inverse Laplace transformations (ILT) expressions of the temperature field and velocity field are too complicated to so solve analytically. As such, we have implemented the ILT for the temperature and velocity profiles numerically using Tzou's algorithm [55] and Zakian's algorithm [56; 58].

Tzou's method [55] is given by

$$w(\xi,t)=\frac{e^{4.7}}{t}\cdot\left[\frac{1}{2}\overline{w}\left(\xi,s\right)+Re\sum_{j=1}^{N}(-1)^{k}\overline{w}\left(r,\frac{4.7+k\pi i}{t}\right)\right], \tag{3.21}$$

while Zakian's method [56] is written as

$$w(\xi,t)=\frac{t}{2}\sum_{j=1}^{N}Re\left[K_j\overline{w}\left(\xi,\frac{\alpha_j}{t}\right)\right], \tag{3.22}$$

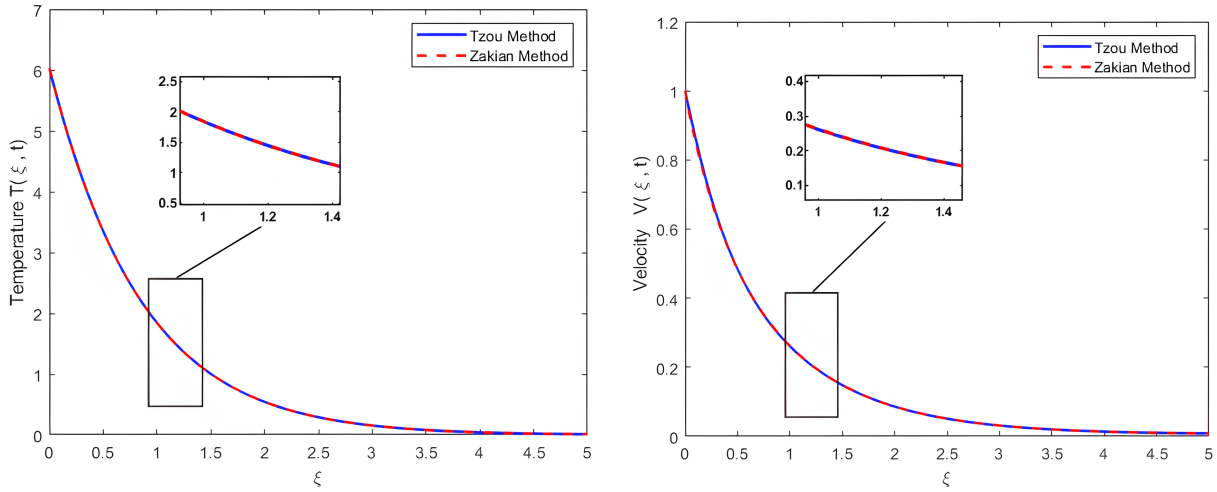
where K_j and α_j are constants and Re denotes the real part of the $\overline{w}\left(\xi,s\right)$ function. To verify our ILT solutions, the output from the two numerical approaches is graphically compared. Notably, the overlapped nature of the plotted results indicates a significant level of agreement between the two methods. This agreement reinforces the confidence in the accuracy and reliability of the inverse Laplace transform calculations performed using these numerical approaches.

3.5 Numerical Results and Discussion

In this chapter, we applied the PBFD to investigate the thermal and velocity dynamics of the aforementioned problem. The problem geometry in this study involves the flow of blood over a permeable vertical plate, with the inclusion of SWCNT and MWCNT nanoparticles, and the presence of thermal radiation, an applied magnetic field, and vibration. The solution of the temperature and momentum profiles are obtained with the use of Laplace transformations, with the ILT computed numerically. The computation was conducted using MATLAB [59]. To observe the effects of different parameters, we fix all parameters and vary only the parameter of interest.

3.5.1 Comparison of Tzou and Zakian numerical schemes

A comparison between the ILT techniques of Tzou and Zakian for the temperature and velocity profiles is illustrated in Figures 3.2a and 3.2b, respectively. Table 3.3 shows some numerical values for the same techniques. The results presented exhibit a good level of accuracy.



(a) (b)

Figure 3.2: Tzou and Zakian method for temperature (a) and velocity (b)

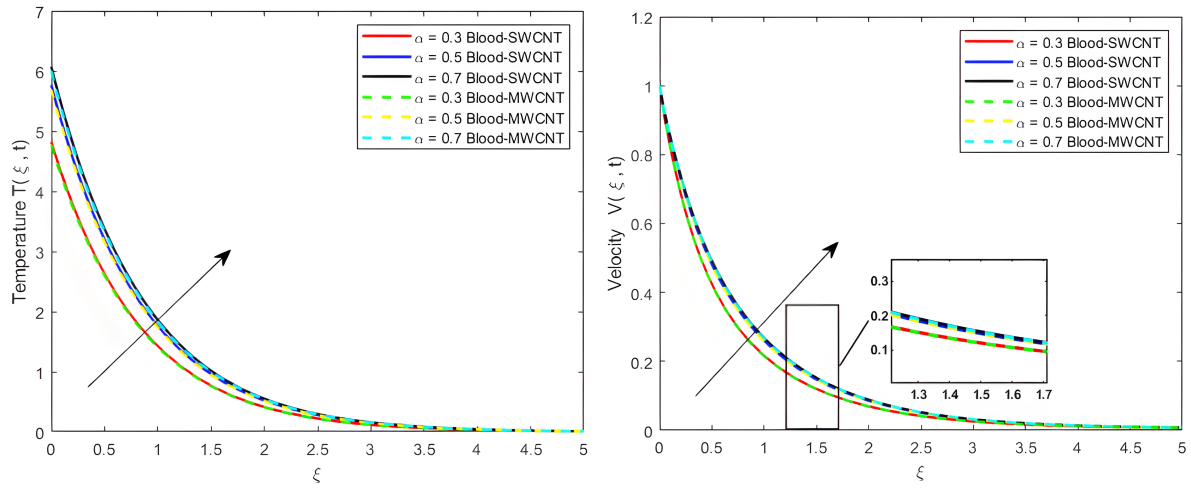
Table 3.3: Evaluation of temperature and velocity distributions using distinct numerical schemes

Parameter	Temperature Profile		Velocity Profile	
xi	Tzou Scheme	Zakian Scheme	Tzou Scheme	Zakian Scheme
0.1	5,3651	5,3684	0,8509	0,8623
0.3	4,2422	4,2445	0,6346	0,6400
0.5	3,3490	3,3503	0,4836	0,4840
0.7	2,6397	2,6403	0,3751	0,3739
0.9	2,0774	2,0776	0,2945	0,2933
1.1	1,6326	1,6325	0,2332	0,2324
1.3	1,2811	1,2809	0,1858	0,1854
1.5	1,0040	1,0036	0,1487	0,1484
1.7	0,7857	0,7854	0,1195	0,1193
1.9	0,6141	0,6138	0,0963	0,0962

3.5.2 Effect of fractional variables α, β and γ

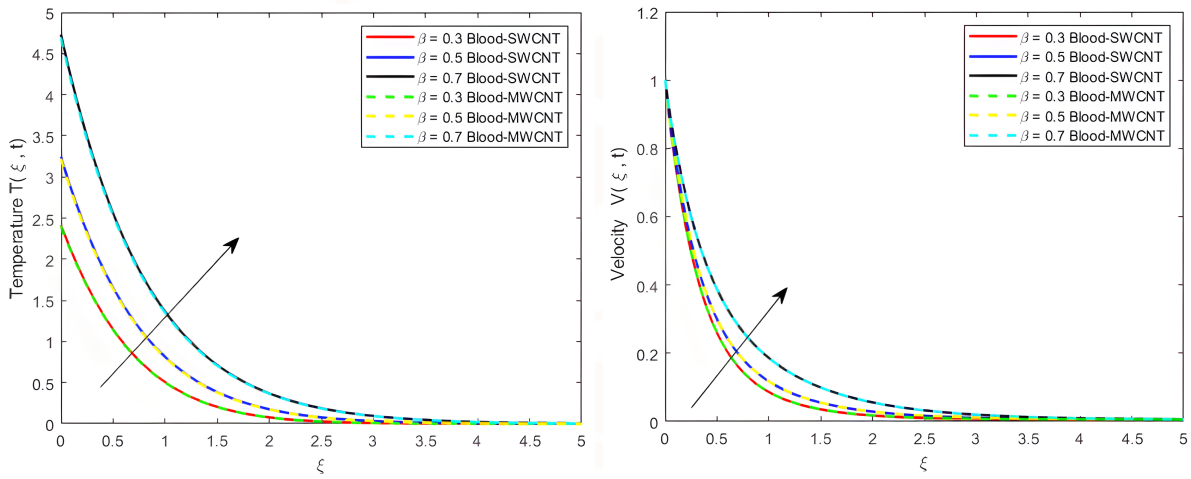
The impact of the fractional parameters α, β, and γ on the temperature and velocity distribution is depicted in Figures (figs. 3.3 to 3.5). For larger values of these fractional parameters, an increase in the temperature profile is observed.

Additionally, it is noteworthy that an increase in these fractional parameters yields a corresponding increase in the velocity profile for both SWCNTs and MWCNTs.



(a) (b)

Figure 3.3: Variation of α on the temperature and velocity fields, while maintaining $\beta = \gamma = 0.8$, Pr $= 3$, Gr $= 3.2$, $\phi = 0.1$, $R = 1.7$ and t $= 0.6$.



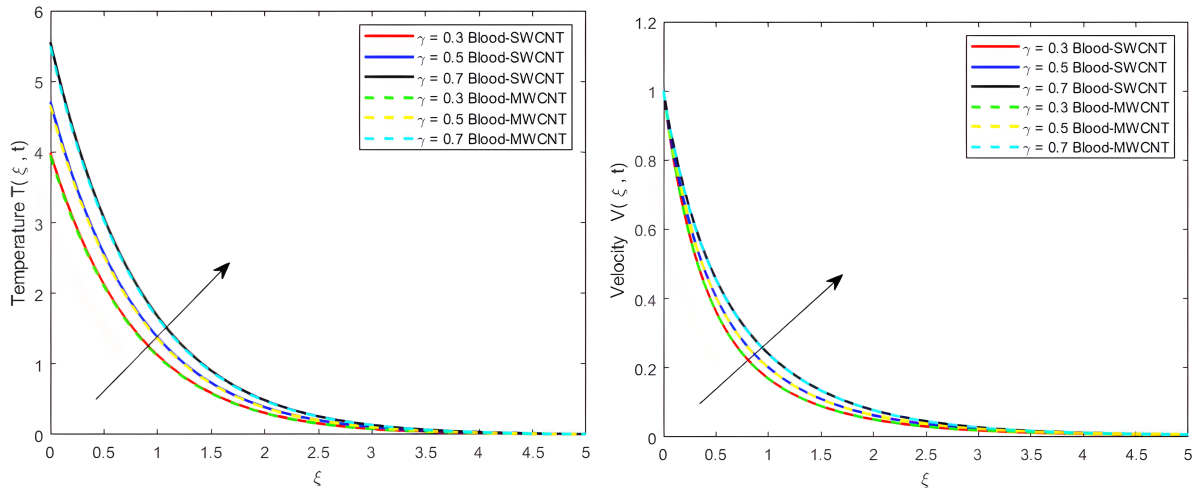
(a) (b)

Figure 3.4: Temperature and velocity distribution influenced by changes in β, in the presence of fixed values for $\alpha = \gamma = 0.8$, Pr $= 3$, Gr $= 3.2$, $\phi = 0.1$, $R = 1.7$ and t $= 0.6$.

3.5.3 Effect of Nanoparticle Volume Fraction ϕ

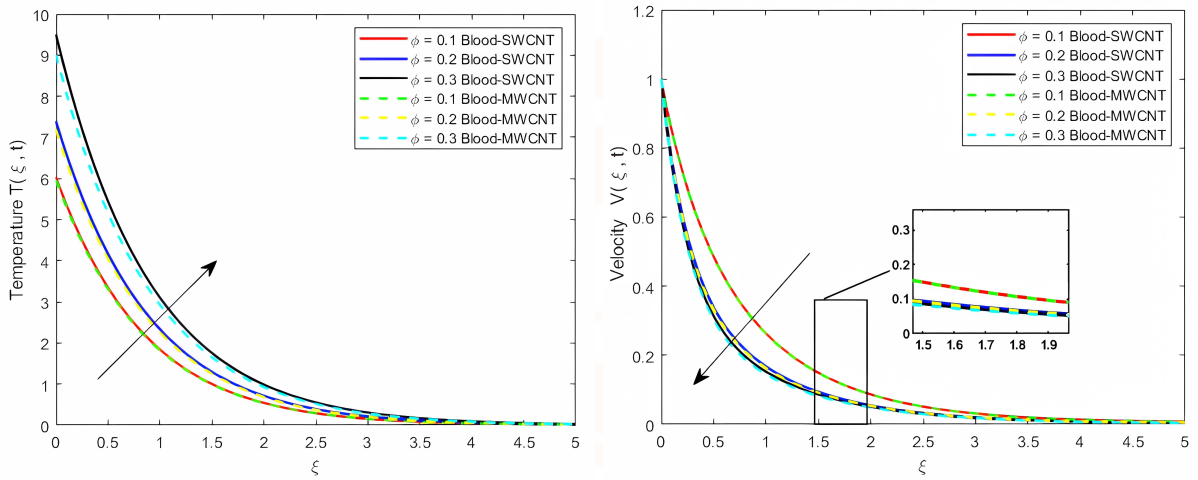
The variation in volume fractions is indicated in Figure 3.6 and its corresponding impact is shown. Figure 3.6a shows that the temperature profile is positively correlated with the volume fraction. An increase in the volume fraction is expected to produce a thicker temperature profile owing to the enhanced interaction among carbon nanotubes.

Figure 3.6b shows the effect of various values of the volume fraction on the velocity profile. It is noted that the velocity profile decays with increase in the volume fraction. The reason behind this behavior can be attributed to the enhanced viscous effect of the NF, resulting in a decline in the velocity profile.



(a) (b)

Figure 3.5: Temperature and Velocity field by variation of γ while maintianing $\alpha = \beta = 0.8$, Pr = 3, Gr = 3.2, $\phi = 0.1$,R= 1.7, $t = 0.6$.



(a) (b)

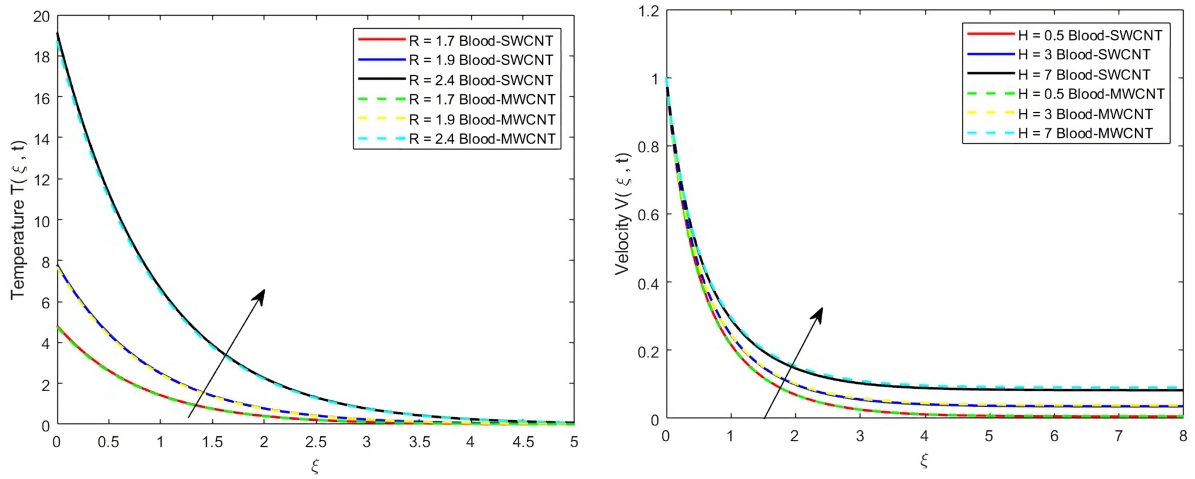
Figure 3.6: Temperature and Velocity field by variation of ϕ with $\alpha = \beta = \gamma = 0.8$, Pr = 3, R = 1.7, Gr = 3.2, t = 0.6

3.5.4 Effect of Radiation parameter R and Vibration

Figures 3.7a and 3.7b show the effect of radiation and vibration on the temperature and velocity profiles, respectively. It is noted that an increase in the radiation parameter leads to a corresponding increase in the temperature profile. This occurs because higher radiation parameters affect the nanofluid's ability to absorb and emit radiation, influencing the temperature profile. Higher radiation parameter imply a greater capacity for the nanofluid to absorb and retain thermal energy, which results in an increased temperature profile.

More vibration in the system leads to an increase in the velocity distribution of the system. The vibrations stimulate fluid flow in a way that enhances the overall velocity of the fluid. Fur-

thermore, the additional energy caused by the vibration increases the overall kinetic energy of the particles in the system, leading to higher velocities.



(a) (b)

Figure 3.7: Effect of Radiation and Vibration on Temperature and Velocity field respectively with $\alpha = \beta = \gamma = 0.8$, Pr = 3, Gr = 3.2, t = 0.6.

3.5.5 Effect of Prandtl Number Pr and Grashof Number Gr

The Prandtl number Pr characterizes the correlation between thermal and momentum diffusion. The effect of different values of Pr is demonstrated in Figures 3.8a and 3.8b. It is noted that for higher values of Pr, the temperature distribution decreases. The higher diffusivity and lower viscosity are likely contributors to this phenomenon, enhancing heat mixing in the fluid and diminishing the overall thermal profile.The velocity profile exhibits an upward trend as the Prandtl Number increases, primarily influenced by the amplified thermal diffusivity.

Figure 3.8c reflects the effect of different values of the Grashof number Gr on the velocity distribution. We notice that for greater values of Gr, the velocity profile increases. This is due to an increase in the buoyancy of the fluid. Both SWCNTs and MWCNTs exhibit this phenomenon.

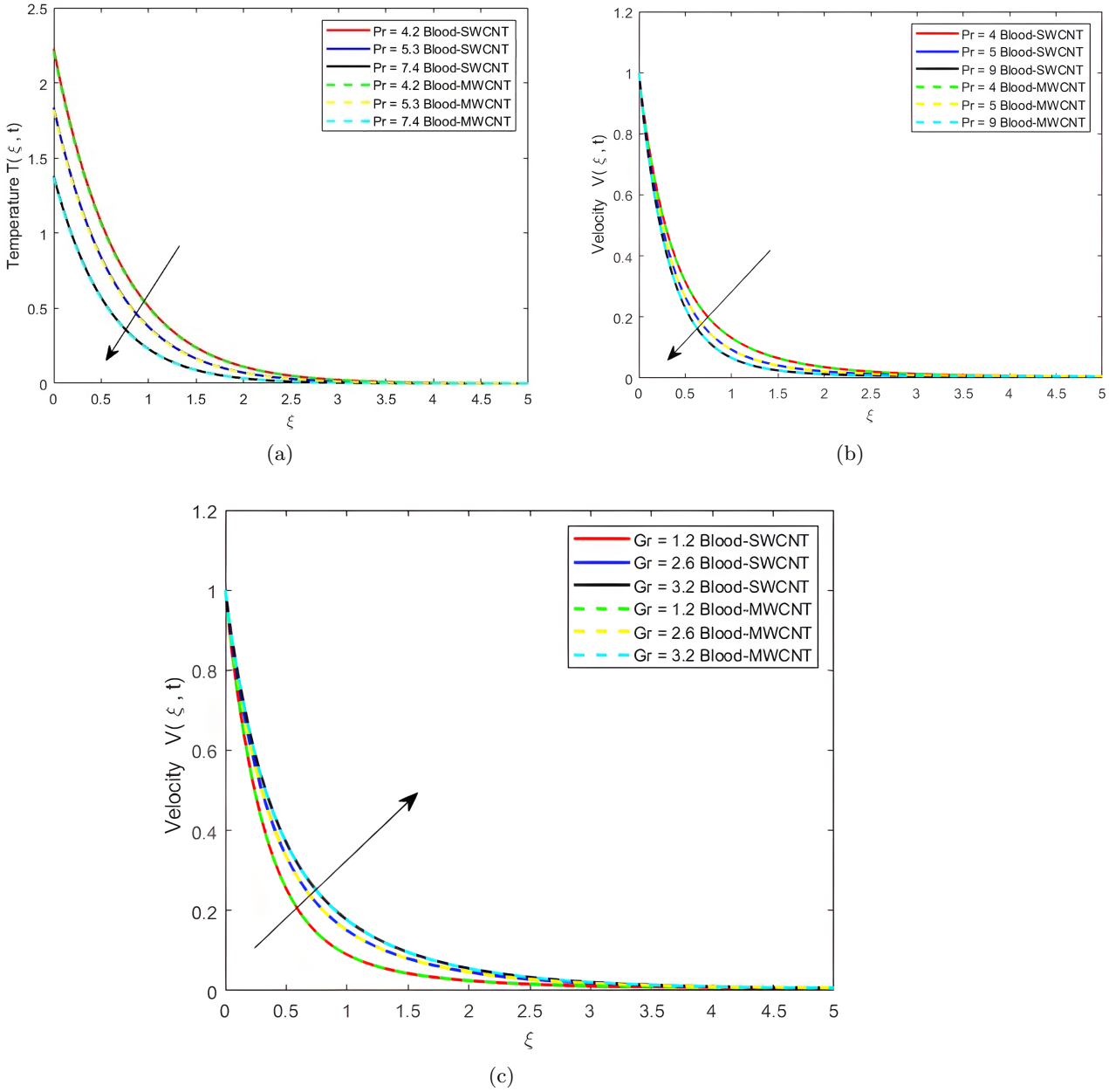


Figure 3.8: Temperature and Velocity fields by variation of Pr and Velocity field by variation of Gr with $\alpha = \beta = \gamma = 0.8$, $\phi = 0.1, t = 0.6, R = 1.7$

3.5.6 Nusselt Number Nu and Skin friction C_f

Given the importance of these physical variables, the Nusselt number (Nu) is utilized to calculate the heat transfer rate, and the skin friction coefficient (C_f) is employed to evaluate the shear stress. These are calculated using the following mathematical relations:

$$Nu = \frac{h\overline{q}}{k_f(T_W - T_\infty)}, \tag{3.23}$$

where

$$\overline{q} = -k_{nf} \frac{\partial T}{\partial \xi}\bigg|_{\xi=0}. \tag{3.24}$$

The skin friction is calculated thus:

$$C_f = \frac{\tau_w}{\frac{1}{2}\rho_f U^2}. \tag{3.25}$$

Tables 3.4 and 3.5 display the calculated values of the Skin friction and Nusselt number, respectively, under varying parameter conditions.

Table 3.4: Skin friction analysis for different parameter values with default values $\alpha = 0.5, \beta = 0.8, \gamma = 0.3, \phi = 0.1, Pr = 3, Gr = 5.2$

α	β	γ	ϕ	Pr	Gr	C_f
0.5	0.8	0.3	0.1	3	5.2	2,73142
0.7						2,70349
0.9						2,71453
	0.4					3,31541
	0.6					3,11527
	0.8					2,70545
		0.3				2,70545
		0.5				2,46196
		0.7				2,16822
			0.11			2,70545
			0.13			3,86605
			0.15			3,12718
				7		2,70545
				9		3,49771
				12		3,58390
					5.3	2,68503
					5.5	2,60332
					5.7	2,56247

Table 3.5: Evaluation of the Nusselt number with default values $\alpha = 0.5, \beta = 0.8, \gamma = 0.3, \phi = 0.1, Pr = 3, Gr = 5.2$

α	β	γ	ϕ	Pr	Gr	Nu
0.5	0.8	0.3	0.1	3	5.2	7,2288
0.7						7,2402
0.9						7,2613
	0.3					7,2403
	0.5					7,2563
	0.7					7,3858
		0.5				7,4346
		0.6				7,4924
		0.7				7,2736
			0.1			7,2683
			0.2			8,2165
				7		7,2724
				9		7,2103

3.6 Conclusions

In this chapter, we studied the flow nature of SWCNT and MWCNT imbedded in blood with radiation and vibration conditions. The Casson fluid model is employed to simulate blood flow. The PBFD was applied on the governing equations. Laplace transform was used to solve the system. Numerical techniques, namely Tzou's and Zakian's schemes, were employed to obtain the ILT numerically. The primary results of our study are as follows.

- Varying the fractional parameters and other parameters affects the temperature and velocity distributions in different ways for both SWCNTs and MWCNTs, by other increasing or decreasing the distributions.
- Thermal radiation causes an overall increase in the temperature profile.
- The temperature and velocity profiles exhibit a downward trend as the fractional parameters increase and approach zero as $\xi \to \infty$, which is in accordance with the boundary conditions.
- The PBFD is a valuable and effective tool for studying the dynamics of the aforementioned problem.

4. Atangana-Baleanu fractional simulation of thermal $Cu - Al_2O_3$/Casson hybrid NF flow with radiation across an oscillating surface considering shape effects

4.1 Introduction

This chapter presents numerical investigations conducted to analyze the flow and heat transfer phenomena of blood HNF containing $Cu - Al_2O_3$ nanoparticles. The mathematical results are presented with consideration of the effects of various important parameters on the temperature and velocity profiles. The Casson fluid model is employed to simulate blood. The inverse Laplace will be computed numerically using Tzou [55] and Zakian [56] schemes.

Considering the aforementioned literature and related articles (Chapter 2), the aims of this chapter are:

- To study the thermal and velocity effects of a blood-based HNF with Copper (Cu) and Aluminium Oxide (Al_2O_3) with radiation and an oscillating plate using fractional calculus.
- To analyze the rheological properties of blood as a base fluid utilizing the Casson fluid model, with a particular emphasis on understanding its shear thinning and shear thickening nature.
- To perform the fractional simulations using the ABFD technique and Laplace transformation approach.
- To analyze how different nanoparticle shapes impact the temperature and velocity profiles.
- To find the solutions by simulating the ILT numerically by applying Tzuo's method and Zakian's method, and analyse the physical interpretations of the results.

4.2 Mathematical Formulation

We consider the flow of Casson HNF over a vertical, permeable and oscillating plate with applied radiative flux. The base fluid utilized in the study is blood, and the nanoparticles employed consist of Copper (Cu) and Aluminium Oxide (Al_2O_3). Furthermore, a magnetic field of intensity B_0 is imposed at an angle of θ. Initially, the temperature of the fluid is at T_w. The fluid's temperature fluctuates from T_w to T_∞ over time, while the plate vibrates with $U_0 H(t) cos(\omega t)$. It is also considered that velocity does not influence the applied radiation. The flow geometry is depicted in Figure 4.1.

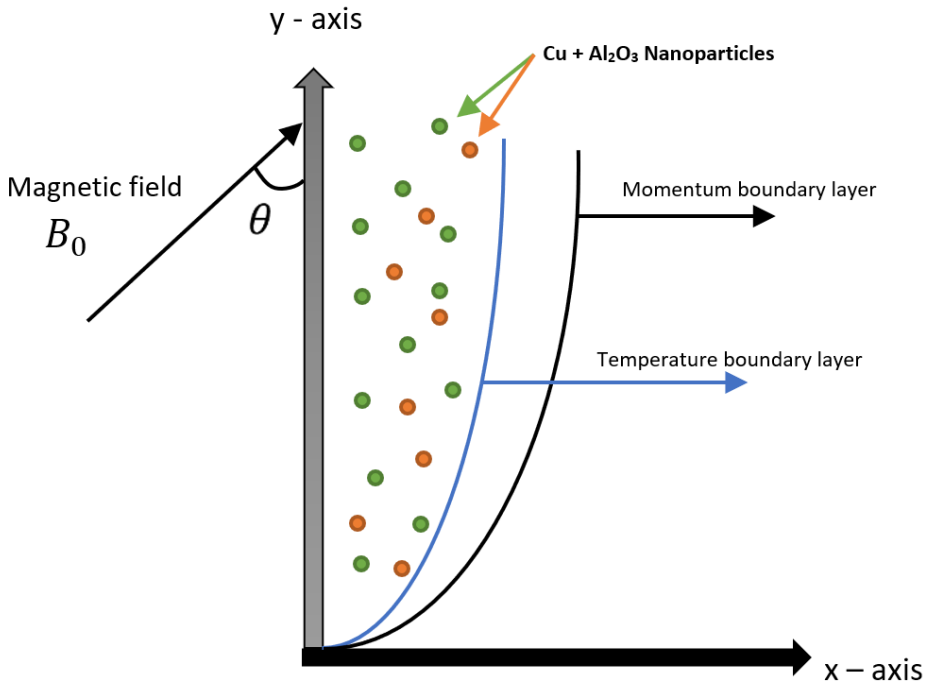


Figure 4.1: Geometry of the problem

Table 4.1: Material Properties of base fluid and nanoparticles

Material	Blood	Cu	Al_2O_3
ρ (kg/m^3)	1053	8933	3970
C_p (J/kgK)	3594	385	765
σ	0.8	5.96×10^{7}	1.502×10^{-10}
k (W/mK)	0.492	400	40

The Casson fluid model [4] is given thus:

$$\tau_{ij} = \begin{cases} 2\left(\mu_B + \frac{p_r}{\sqrt{2\pi_c}}\right) e_{ij}, & \text{if } \pi < \pi_c, \\ 2\left(\mu_B + \frac{p_r}{\sqrt{2\pi}}\right) e_{ij}, & \text{if } \pi > \pi_c. \end{cases} \tag{4.1}$$

The symbols p_r, μ_B, and π_c represent the yield stress, plastic dynamic viscosity, and the product of μ_B and p_r respectively. Table (4.1) outlines the material attributes of both the base fluid and nanoparticles.

Table (4.2) provides the thermophysical properties of NFs, while Table (4.3) presents the properties of HNFs.

Table 4.2: Thermophysical properties of NFs

Quantity	Relation
Dynamic Viscosity	$\mu_{nf} = \mu_f(1-\phi)^{-2.5}$
Thermal Expansion	$(\rho\beta_T)_{nf} = (1-\phi)(\rho\beta_T)_f + \phi(\rho\beta_T)_s$
Heat Capacitance	$(\rho C_p)_{nf} = (1-\phi)(\rho C_p)_f + \phi(\rho C_p)_s$
Thermal Conductivity	$k_{nf} = k_f \frac{(k_s - 2\phi(k_f - k_s) + 2k_f)}{(k_s + 2\phi(k_f - k_s) + 2k_f)}$
Electrical Conductivity	$\frac{\sigma_{nf}}{\sigma_f} = 1 + \left\{3\left(\frac{\sigma_s}{\sigma_f} - 1\right)\phi\right\}\left\{\left(\frac{\sigma_s}{\sigma_f} + 1\right) - \left(\frac{\sigma_s}{\sigma_f} - 1\right)\phi\right\}^{-1}$

Table 4.3: Thermophysical properties of HNFs

Quantity	HNF
Dynamic Viscosity	$\mu_{hnf} = \mu_f(1-\phi_1)^{-2.5}(1-\phi_2)^{-2.5}$
Thermal Expansion	$(\rho\beta_p)_{hnf} = (1-\phi_2)[(1-\phi_1)\rho\beta_p)_f + \phi_1(\rho\beta_p)_{n1}] + \phi_2(\rho\beta_p)_{n2}$
Heat Capacitance	$(\rho C_p)_{hnf} = (1-\phi_2)[(1-\phi_1)\rho C_p)_f + \phi_1(\rho C_p)_{n1}] + \phi_2(\rho C_p)_{n2}$
Thermal Conductivity	$\frac{k_{hnf}}{k_f} = \frac{k_{n2} + (m-1)k_{bf} - (m-1)\phi_2(k_{bf} - k_{n2})}{k_{n2} + (m-1)k_{bf} + \phi_2(k_{bf} - k_{n2})}$
Electrical Conductivity	$\frac{\sigma_{hnf}}{\sigma_f} = 1 + \frac{3\phi\left(\phi_1\sigma_1 + \phi_2\sigma_2 - \sigma_{bf}(\phi_1 + \phi_2)\right)}{\phi_1\sigma_1 + \phi_2\sigma_2 + 2\phi\sigma_{bf} - \phi\sigma_{bf}\left(\phi_1\sigma_1 + \phi_2\sigma_2 - \sigma_{bf}(\phi_1 + \phi_2)\right)}$, $\phi = \phi_1 + \phi_2$

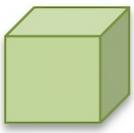
Particle Form	***Shapes***	***Shape factor (m)***
Bricks		3.7
Cylinder		4.9
Platelet		5.7
Blade		8.9

Figure 4.2: Values of m corresponding to the different shapes of nanoparticles

Expressed below are the governing equations for the model:

- Momentum Equation

$$\rho_{hnf}\frac{\partial v^*}{\partial t^*} = \mu_{hnf}\left(1+\frac{1}{\beta_0}\right)\frac{\partial^2 v^*}{\partial \xi^{*2}} - \left(\sigma_{hnf}B_0^2 sin\theta + \left(1+\frac{1}{\beta_0}\right)\frac{\mu_{hnf}\phi}{\kappa}\right)v^* + g(\rho B_T)_{hnf}(T^*-T_\infty), \tag{4.2}$$

- Energy Equation

$$(\rho C_p)_{hnf}\frac{\partial T^*(\xi^*,t^*)}{\partial \xi^*} = -\frac{\partial q^*(\xi^*,t^*)}{\partial \xi^*}, \tag{4.3}$$

- Radiative Heat Flux

$$q^* = -\frac{4\sigma^*}{3k^*}\frac{\partial}{\partial \xi}T^{*4}_{(\xi^*,t^*)}, \tag{4.4}$$

with the IC and BC set as:

$$\begin{aligned} &v^*(\xi^*,0) = 0, && T^*(\xi^*,0) = T_\infty, \quad \forall \xi^* \geq 0, \\ &v^*(0,t^*) = U_0 H(t^*)cos(\omega t^*), && T^*(0,t^*) = T_W, \quad t^* > 0, \\ &v^*(\xi^*,t^*) \to 0, && T^*(\xi^*,t^*) \to 0, \quad \xi^* \to \infty, t^* > 0. \end{aligned} \tag{4.5}$$

The dimensionless variables are defined in the following way:

$$\begin{aligned} &v^* = \frac{v}{v_0}, && \xi^* = \frac{v_0}{v_f}\xi, \quad t^* = \frac{v_0^2}{v_f}t, \\ &T^* = \frac{T_{(\xi,t)}-T_\infty}{T_W - T_\infty}, && q^* = \frac{q}{q_0}, \quad q_0 = k_f\frac{(T_W-T_\infty)v_0}{v_f}. \end{aligned} \tag{4.6}$$

Using these variables, and expanding T^{*4} about T_∞ while ignoring the higher order terms and subsequently dropping the * symbol, the above equations become:

$$\eta_0\frac{\partial v_{(\xi,t)}}{\partial t} = \frac{\eta_1}{\beta_1}\frac{\partial^2 v_{(\xi,t)}}{\partial \xi^2} - \left(\eta_2 M Sin\theta + \frac{\eta_1}{\kappa}\right) + \eta_3 Gr T_{(\xi,t)}, \tag{4.7}$$

$$\eta_4 Pr\frac{\partial T_{(\xi,t)}}{\partial t} = -\eta_5\frac{\partial q_{(\xi,t)}}{\partial \xi}, \tag{4.8}$$

$$q_{(\xi,t)} = -R\frac{\partial T_{(\xi,t)}}{\partial \xi}, \tag{4.9}$$

accompanied by the relevant IC and BC:

$$\begin{aligned} v(\xi,0) &= 0, & T(\xi,0) &= 0, & \forall \xi \geq 0 \\ v(0,t) &= H(t)cos(\omega t), & T(0,t) &= 1, & t > 0, \\ v(\xi,t) &\to 0, & T(\xi,t) &\to 0, & \xi \to \infty, t > 0, \end{aligned} \tag{4.10}$$

where

$$M = \frac{v_f \sigma_f B_0^2}{\rho_f v_o^2}, \qquad R = -\frac{16\sigma^* T_\infty^3}{3k^*}, \qquad \beta_1 = \frac{\beta_0}{1+\beta_0},$$
$$Pr = \left(\frac{\mu C_p}{\kappa}\right)_f, \qquad k = \frac{\kappa v_o^2}{v_f \phi}, \qquad Gr = \frac{g(\rho B_t)_f (T_W - T_\infty)}{\nu^3}.$$

The constants above represent the Magnetic number (M), Radiation parameter (R), Casson fluid parameter (β_1), Prandtl number (Pr), permeability constant k, and Grashof number (Gr).

The constants $\eta_0, \eta_1, \eta_2, \eta_3, \eta_4$, and η_5 are related to the volume fraction of the nanoparticles, and are defined as:

$$\eta_0 = \frac{\rho_{hnf}}{\rho_f}, \qquad \eta_1 = \frac{1}{(1-\phi_1)^{2.5}(1-\phi_2)^{2.5}}, \qquad \eta_2 = \frac{\sigma_{hnf}}{\sigma_f},$$
$$\eta_3 = \frac{(\rho B_T)_{hnf}}{(\rho B_T)_f}, \qquad \eta_4 = \frac{(\rho C_p)_{hnf}}{(\rho C_p)_f}, \qquad \eta_5 = \frac{k_{hnf}}{k_f}.$$

4.3 Atangana-Baleanu Fractional Order

The ABFD is implemented

$$q_{(\xi,t)} = -{}^{AB}\mathfrak{D}_t^\beta R \frac{\partial T}{\partial \xi}, \tag{4.11}$$

where ${}^{AB}\mathfrak{D}_t^\beta$ is the ABFD [7], which is defined:

$${}^{AB}\mathfrak{D}_t^\beta h_{(\xi,t)} = \frac{1}{1-\beta}\int_0^t E_\beta \left[-\frac{\beta(\tau-t)^\beta}{1-\beta}\right] \frac{\partial h_{(\xi,t)}}{\partial \tau} d\tau, \quad 0 \leq \beta \leq 1,$$

where

$$E_\beta(-t^\beta) = \sum_{m=0}^{\infty} \frac{(-t)^{\beta m}}{\Gamma(\beta m + 1)}.$$

The Laplace of the Atangana-Baleanu operator ${}^{AB}\mathfrak{D}_t^{\beta}$ is implemented as:

$$\mathcal{L}[{}^{AB}\mathfrak{D}_t^{\beta}] = \frac{s^{\beta}\mathcal{L}(h_{(\xi,t)}) - h(\xi,0)}{(1-\beta)s^{\beta}+\beta}; \quad 0 \leq \beta \leq 1. \tag{4.12}$$

4.4 Solution of the problem

4.4.1 Solution of the temperature profile [Equations (4.8) and (4.11)]

For the solution to the temperature profile, taking the Laplace transformations of equations (4.8) and (4.11) and on its accompanying conditions, we get

$$\eta_4 Pr s\overline{T}_{(\xi,t)} = -\eta_5 \frac{\partial \overline{q}_{(\xi,t)}}{\partial \xi}, \tag{4.13}$$

$$\overline{q} = \frac{s^{\beta}\overline{T}}{(1-\beta)s^{\beta}+\beta} R \frac{\partial \overline{T}_{(\xi,t)}}{\partial \xi}, \tag{4.14}$$

Introducing (4.14) to (4.13) we obtain the differential equation

$$\frac{\partial^2 \overline{T}_{(\xi,t)}}{\partial \xi^2} - \frac{\eta_4 Pr}{\eta_5 R}\frac{s^{\beta}}{(1-\beta)s^{\beta}+\beta}\overline{T} = 0. \tag{4.15}$$

By imposing the initial conditions, we derive the solution to (4.15) as:

$$\overline{T}_{(\xi,s)} = \frac{1}{s} e^{-\xi\sqrt{\frac{\eta_4 Pr}{\eta_5 R}\frac{s^{\beta}}{(1-\beta)s^{\beta}+\beta}}}, \tag{4.16}$$

where $\overline{T}$ is the solution of the temperature in the s-domain.

4.4.2 Solution of the velocity profile [Equation (4.7)]

Upon applying Laplace transformations to (4.7) in conjunction with the respective IC and BC, we derive the following non-homogeneous differential equation:

$$\frac{\partial^2 \overline{v}_{(\xi,s)}}{\partial \xi^2} - \left(\frac{l_4 s^{\beta}+l_5}{s^{\beta}+l_2}\right)\overline{v}_{(\xi,s)} = -\eta_3 \overline{T}_{(\xi,s)}, \tag{4.17}$$

where

$$l_0 = \frac{B\eta_0}{\eta_1(1-\beta)}, \qquad l_1 = \frac{\eta_4 Pr}{\eta_5(1-\beta)},$$
$$l_2 = \frac{\beta}{1-\beta}, \qquad l_3 = \frac{\beta_1\eta_3 Gr}{\eta_1},$$
$$l_4 = \frac{\beta_1\eta_2}{\eta_1}MSin\gamma + \frac{\beta_1}{k} + l_0, \qquad l_5 = l_2\left(\frac{\beta_1\eta_2}{\eta_1} + \frac{\beta_1}{k}\right).$$

Equation (4.17) has the solution

$$\overline{v}_{(\xi,s)} = \frac{s}{s^2+\omega^2}e^{-\sqrt{\frac{l_4 s^\beta + l_5}{s^\beta + l_2}}} + \frac{l_3(s^\beta + l_2)}{s((l_1 - l_4)s^\beta - l_5)}\left(e^{-\xi\sqrt{\frac{l_4 s^\beta + l_5}{s^\beta + l_2}}} - e^{-\xi\sqrt{\frac{l_1 s^\beta}{s^\beta + l_2}}}\right). \tag{4.18}$$

The inverse Laplace transformations were implemented numerically using Tzou's [55] and Zakian's algorithms [56; 58].
Tzou's method is given by

$$w(\xi,t) = \frac{e^{4.7}}{t}\cdot\left[\frac{1}{2}\overline{w}(\xi,s) + Re\sum_{j=1}^{N}(-1)^k\overline{w}\left(r, \frac{4.7 + k\pi i}{t}\right)\right], \tag{4.19}$$

while Zakian's method is written as

$$w(\xi,t) = \frac{t}{2}\sum_{j=1}^{N} Re\left[K_j\overline{w}\left(\xi, \frac{\alpha_j}{t}\right)\right], \tag{4.20}$$

where K_j and α_j are constants and Re denotes the real part of the $\overline{w}(\xi,s)$ function.

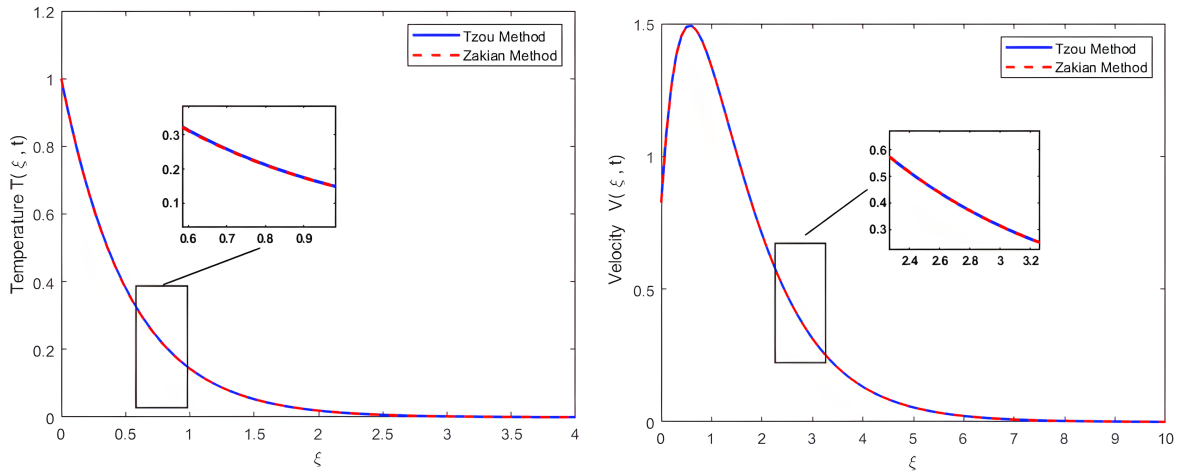
4.5 Numerical Results and Discussion

This study utilized the ABFD to examine the thermal and velocity dynamics of a system consisting of blood flowing over a vertical plate with copper (Cu) and aluminium-oxide (Al_2O_3) nanoparticles, exposed to thermal radiation, a magnetic field, and vibration on the wall. We obtained the thermal and momentum profiles using Laplace transformations and numerically computed the inverse Laplace using Tzou and Zakian schemes. Our simulations involved holding all parameters constant except for the one being studied, in order to observe the effects of varying that particular parameter.

4.5.1 Comparison of numerical schemes

To verify our solutions, the output from the two numerical approaches is graphically compared. The overlap between the results from the two methods demonstrates the accuracy of our solutions. The numerical solutions obtained are depicted as graphs. In Figures 4.3a and 4.3b we

show a comparison between Tzou and Zakian techniques for the inverse Laplace for the temperature and velocity profile respectively. Table 4.4 shows some numerical values for the same techniques. The stated results have good accuracy.



(a) (b)

Figure 4.3: Comparison of numerical schemes with Tzou and Zakian method for temperature (a) and velocity (b)

Table 4.4: Comparative study of temperature and velocity profiles using different numerical approaches

Parameter	**Temperature Profile**		**Velocity Profile**	
ξ	**Tzou Scheme**	**Zakian Scheme**	**Tzou Scheme**	**Zakian Scheme**
0.1	0.8246	0.8265	1.0815	1.0816
0.3	0.5603	0.5630	1.3816	1.3818
0.5	0.3801	0.3822	1.4873	1.4876
0.7	0.2574	0.2588	1.4743	1.4747
0.9	0.1740	0.1748	1.3927	1.3931
1.1	0.1174	0.1178	1.2753	1.2757
1.3	0.0790	0.0792	1.1430	1.1433
1.5	0.0531	0.0532	1.0086	1.0090
1.7	0.0356	0.0357	0.8799	0.8802
1.9	0.0238	0.0239	0.7610	0.7612

4.5.2 Effect of fractional parameter β

Figure 4.6a (top) illustrates the impact of the fractional parameter β on the temperature distribution. As the fractional parameter increases, the thermal profile for both the NF and HNF is seen to decrease. The fluid retains a greater memory of its previous temperature distributions and thermal behavior. This memory effect leads to a dampening effect on the temperature variations and a decrease in the temperature profile. In Figure 4.6b (bottom), the velocity profile is depicted, illustrating the impact of the fractional parameter β. An inverse correlation between the velocity profile and β is observed, suggesting a decrease in velocity as β increases. The memory effect of the fractional paramenter affects the momentum conservation, resulting in a gradual reduction in the velocity profile along the flow direction.

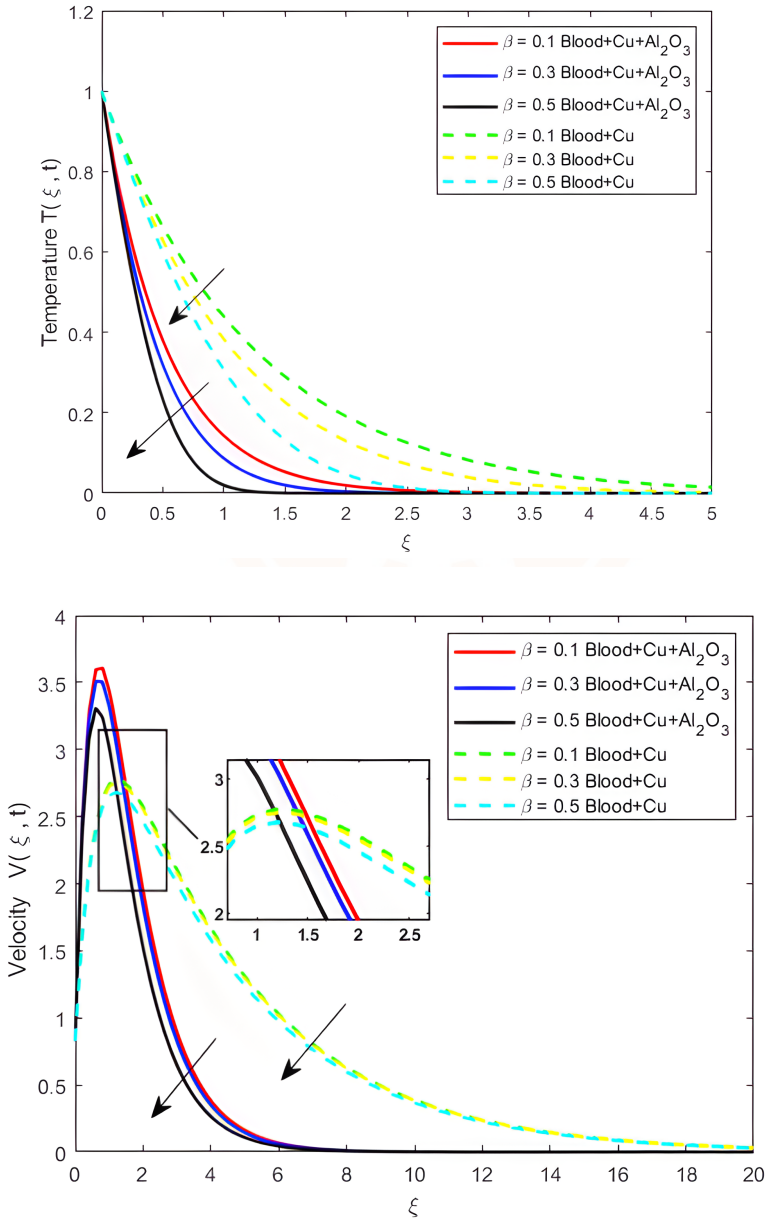


Figure 4.6: Temperature and Velocity field by variation of β with Pr=3, $\theta = \pi/4$, $\phi_{Cu} = \phi_{Al_2O_3} = 0.09$, $R = 1.7$, M=0.5, $t = 0.6$.

4.5.3 Effect of Prandtl Number Pr and Magnetic Parameter M

The effect of different values of the Prandtl number is denoted in Figures 4.7a and 4.7b. It is noted that increasing the Prandtl number results in an decrease in the temperature profile. This is likely due to a higher diffusivity and lower viscosity which can result in a more efficient mixing of heat within the fluid and a decrease in the overall thermal profile. As the Pr number rises, the velocity profile shows a corresponding increase, primarily influenced by the heightened thermal diffusivity of the fluids.

The velocity distribution represented in Figures 4.7c, highlights the effects of different magnetic parameter values (M) on the flow behavior. It is evident that larger values of M lead to a reduction in the velocity profile.

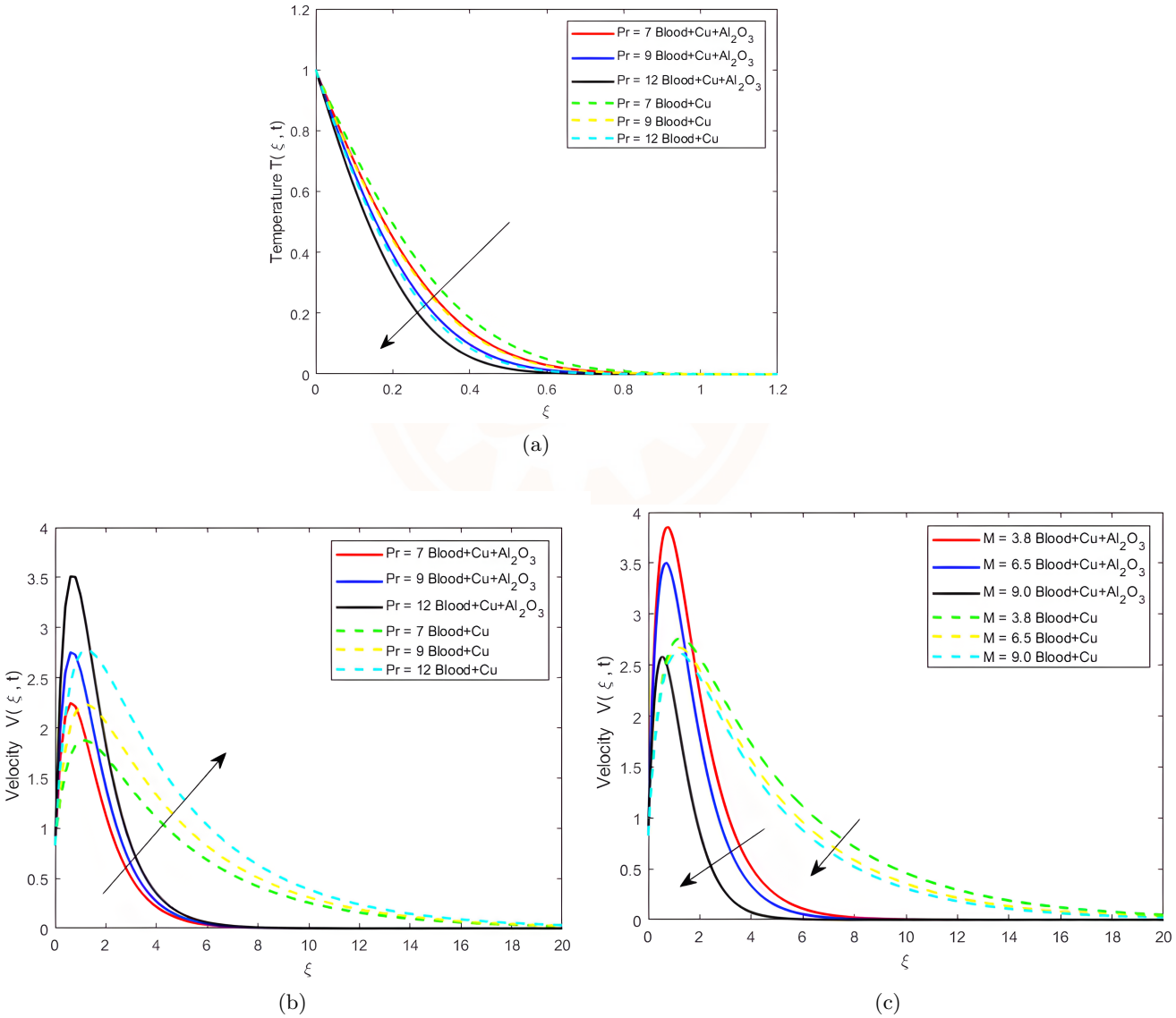
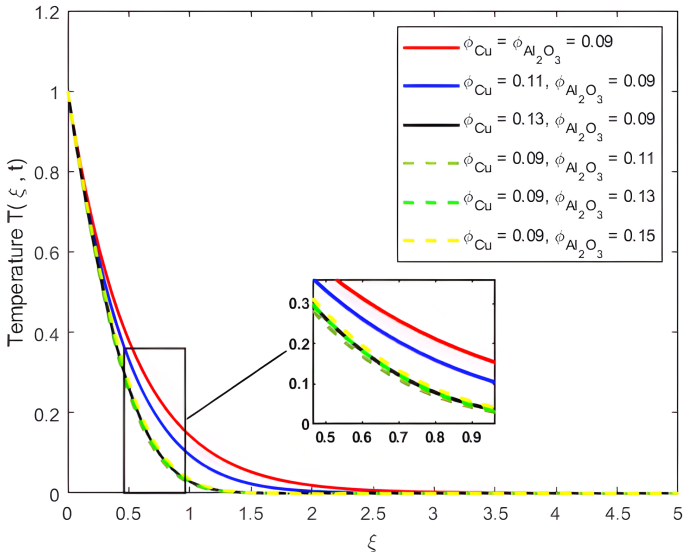


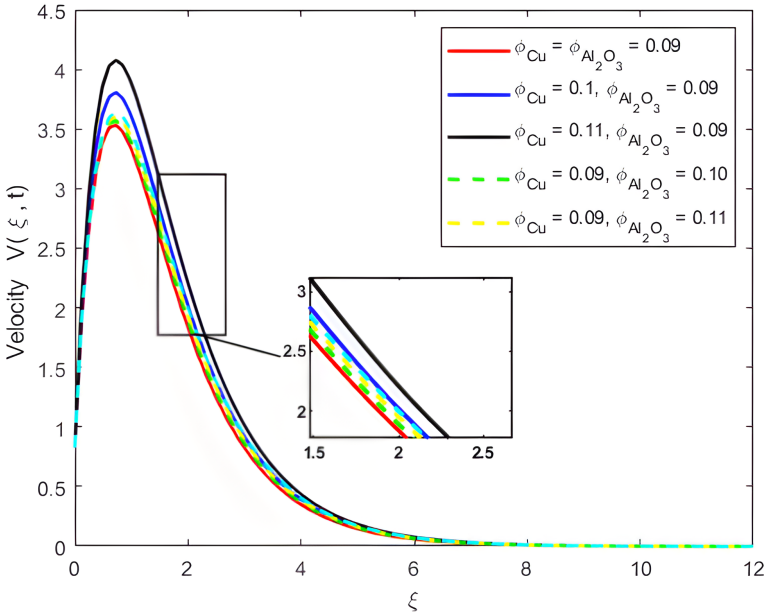
Figure 4.7: Influence of Pr and M on the temperature and velocity profile with $\phi_{Cu} = \phi_{Al_2O_3} = 0.09, \beta = 0.8, \theta = \pi/4$,R= $1.7, t = 0.6$.

4.5.4 Effect of Nanoparticle Volume Fraction ϕ

The effects of various volume fractions are shown in Figure 4.8. A higher volume fraction of copper in the HNF is linked with an decreased temperature profile. This can be attributed to increased thermal conductivity and heat transfer rate of the HNF. The velocity profile exhibits a diminishing trend as the volume fraction increases. The presence of nanoparticles leads to an increased viscosity of the mixture, which is a likely cause of this phenomenon.



(a)



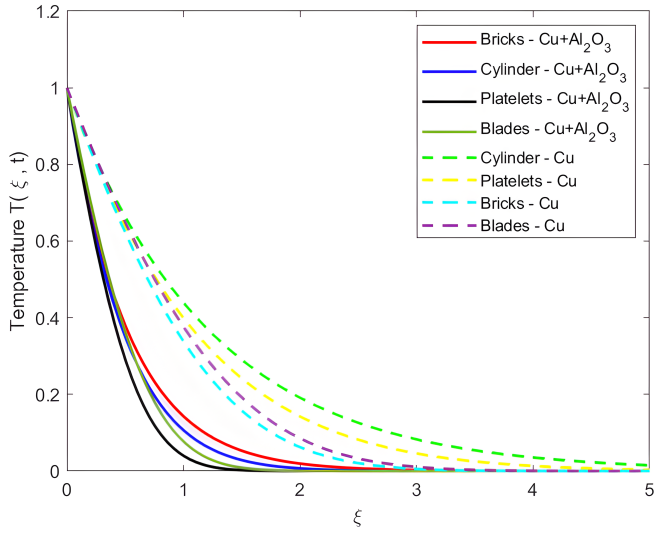
(b)

Figure 4.8: Temperature and Velocity distribution by variation of volume fractions with $\beta = 0.8, Pr = 3$,R= $1.7, t = 0.6$

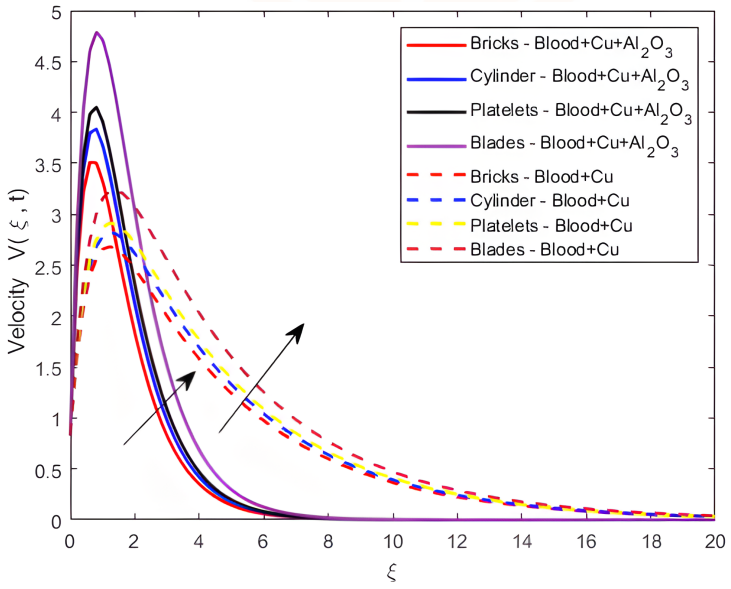
4.5.5 Impact of the shape of the nanoparticles

Figures 4.9a, 4.9b, demonstrate the effect of the shape of the nanoparticles on temperature and velocity profiles, respectively. It is worth noting that Platelet shaped nanoparticles have the lowest temperature profile for the Cu-Al_2O_3 / blood HNF. The presence of platelet-shaped nanoparticles with their larger surface area enhances the heat transfer coefficient and facilitates efficient heat mixing within the blood, giving rise to the observed effect.

Observations show that brick-shaped nanoparticles generate the lowest velocity profiles for both Cu and Cu-Al_2O_3/blood HNF. This could be attributed to higher flow resistance of brick shaped nanoparticles as compared to other shapes, leading to lower velocity profiles.



(a)



(b)

Figure 4.9: Temperature and Velocity distribution by variation of shape factor (m) for $\beta = 0.8 and Pr = 3, Gr = 5.2, M = 0.5, \phi_{Cu} = \phi_{Al_2O_3} = 0.09, \theta = \pi/4$,R= $1.7, t = 0.6$

4.5.6 Effect of Radiation parameter R

Figure 4.10 depicts the effect of thermal radiation on the temperature distribution of both the NF and HNF systems. With higher values of the radiation parameter, a corresponding increase in the temperature in noted. This is due to the system's increased capacity to absorb and retain thermal energy due to applied radiation, which leads to higher thermal profiles.

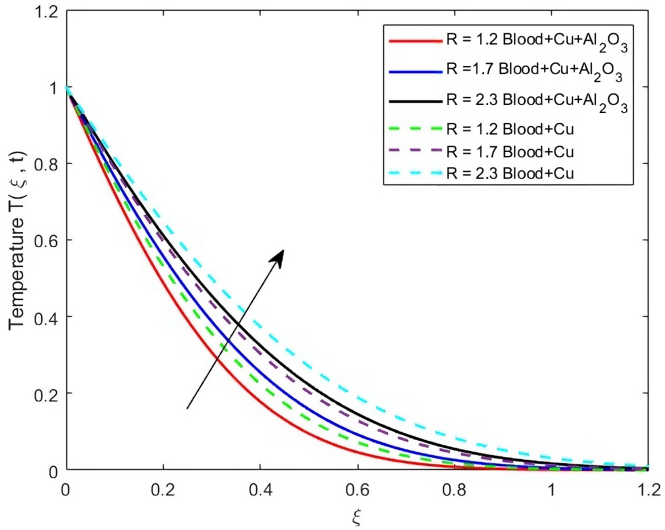
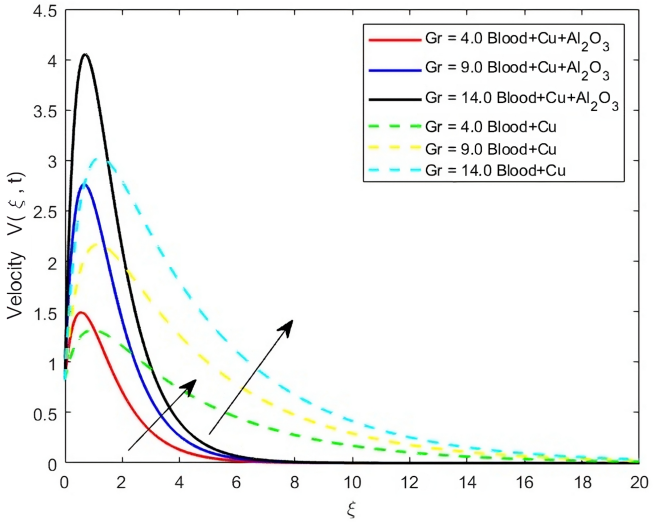


Figure 4.10: Temperature distribution by variation of radiation parameter R for $\beta = 0.8$ and Pr = 3, Gr = 5.2, M = 0.5, $\phi_{Cu} = \phi_{Al_2O_3} = 0.09, \theta = \pi/4, t = 0.6$

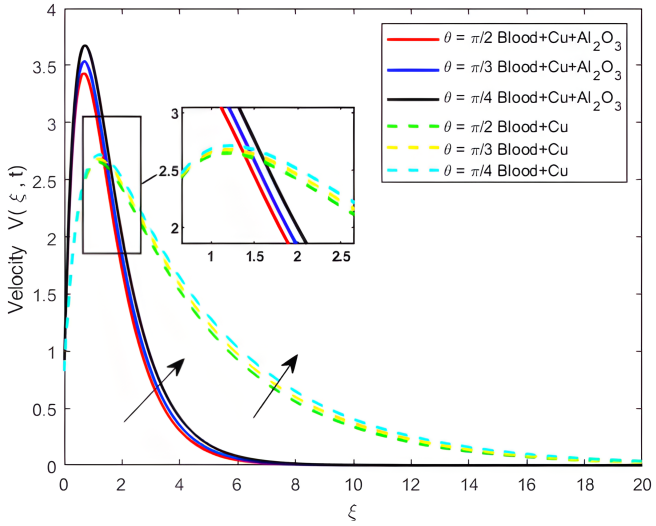
4.5.7 Effect of Grashof Number Gr and Angle θ

The velocity profile's response to variations in the Grashof number Gr and angle θ is depicted in Figures 4.11a and 4.11b, respectively. A higher Grashof number is associated with an increased velocity profile, indicating enhanced fluid flow. The reason behind this behavior is that as the Grashof number increases, the buoyancy force becomes more dominant compared to the viscous force. As such, an increase of the Grashof number leads to a corresponding increase in temperature and concentration gradient, which causes an increase in the velocity profile.

On the other hand, it is observed that decreasing the angle results in a slight increase in the velocity distribution.



(a)



(b)

Figure 4.11: Velocity field by variation of Gr and θ for Pr $= 3$, $\beta = 0.8$, $\phi_{Cu} = \phi_{Al_2O_3} =$ 0.09,R$= 1.7, t = 0.6$

4.5.8 Nusselt Number Nu and Skin Friction C_f

Recognizing the importance of these physical parameters, the Nusselt number (Nu) is employed to calculate the rate of heat transfer, while the skin friction coefficient (C_f) is used to determine the shear stress. These are calculated using the following mathematical relations:

$$Nu = \frac{h\overline{q}}{k_f(T_W - T_\infty)}, \tag{4.21}$$

where

$$\overline{q} = -k_{nf}\frac{\partial T}{\partial \xi}\bigg|_{\xi=0}. \tag{4.22}$$

The skin friction is calculated thus:

$$C_f = \frac{\tau_w}{\frac{1}{2}\rho_f U^2}. \tag{4.23}$$

The Skin friction and Nusselt number outcomes for various values of the fractional parameter β and nanoparticle shapes can be observed in Tables 4.5 and 4.6, respectively.

Table 4.5: Assessment of the skin friction for the NF and HNF

β	$\phi_1 = \phi_2$	Pr	Gr	shape	Casson + Cu	Casson + Cu + Al_2O_3
0.3	0.09	5	13	Brick	1.3288	2.1589
0.5					1.5402	2.2916
0.7					1.8613	2.6460
0.5	0.09	5	13	Cylinder	1.7831	3.1363
				Platelets	1.6336	2.8864
				Blades	1.2181	2.6359

Table 4.6: Evaluation of the Nusselt number for the NF and HNF

β	$\phi_1 = \phi_2$	Pr	shape	Casson + Cu	Casson + Cu + Al_2O_3
0.3	0.09	5	Brick	8,0624	9,1251
0.5				8,0995	9,2062
0.7				8,1620	9,3420
0.5	0.09	5	Cylinder	8,0721	9,0748
			Platelets	7,9144	8,2194
			Blades	8,1851	8,9941

4.6 Conclusions

Our research in this chapter focused on studying the thermal flow properties of Cu/blood NF and Cu-Al_2O_3/blood HNF flowing over an oscillating plate, in the presence of thermal radiation. Blood behavior was simulated using the Casson fluid model. The ABFD was applied on the governing equations. Laplace transform was used to solve the system. We also studied the effects of different shapes of the nanoparticles. Different inverse approaches are used to numerically compare and show the effects of various parameters with changed values for the temperature and velocity profiles. Numerical methods based on Tzou's and Zakian's schemes were used to obtain the inverse Laplace transform. The major deductions from this work are the following.

- Varying the fractional parameter β affects the temperature profiles for both Cu and $Cu - Al_2O_3$/blood HNF. In both cases, increasing the fractional parameter decreases the temperature profile and velocity profile.
- Platelet shaped nanoparticles result in the lowest temperature profile, but brick shaped nanoparticles result in the lowest velocity profile.
- Increasing the Prandtl number causes a reduction in the temperature profile and a simultaneous rise in the velocity distribution.

- Variations in the fractional parameters lead to a decrease in both the temperature and velocity distributions, eventually approaching zero as ξ approaches infinity. These observations align with the specified boundary conditions.
- Comparison of the ILT numerical schemes shows an overlap of Tzou's and Zakian's method certifies the accuracy of the obtained results.

5. Conclusions & Future Scope

5.1 Conclusions

In this thesis, we used fractional order calculus to study the flow characteristics of SWCNT-MWCNT/Casson NF and $Cu - Al_2O_3$/Casson HNFs over vertical plate with radiation and vibration conditions.

In the first chapter, the fundamental conservation laws of bio-fluid dynamics, as well as the definitions of important fluid parameters, are presented. The chapter also briefly introduces fractional order calculus. The second chapter studies the dynamics of blood NF with Single-wall carbon nanotube and Multi-wall carbon nanotubes (SWCNTs and MWCNTs) as the nanoparticles. The Prabhakar fractional derivative is applied. The influence of various parameters on the temperature and velocity profiles is reflected through graphs. In general it is observed that the fractional parameters of the Prabhakar function have effects on the temperature and velocity profiles. An increase in the fractional parameters leads to an increased temperature profile, and a corresponding increase in the velocity distribution. The temperature profile is positively correlated with the volume fraction, whereas an increase in viscosity of the NF due to the presence of nanoparticles leads to a decrease in the velocity distribution. Meanwhile, higher values of the Prandtl number cause a decline in the velocity profile due to an increase in the thermal diffusivity. Effects of the Grashof number are also observed and noted. Higher values result in an increased velocity profile because of the increased buoyancy of the fluid. Higher values lead to an increased temperature profile as a result of the heat introduced into the system. The velocity distribution showed an increase with a corresponding increase in the vibration.

In the third chapter, the Atangana-Baleanu fractional derivative is applied and used to study the flow of blood HNF. The nanoparticles used are Copper (Cu) and Aluminium Oxide (Al_2O_3). The temperature and velocity profiles of the $Cu - Al_2O_3$ HNFs are compared with those of just Cu-blood NF. High values of the fractional variable β are associated with a decrease in both the temperature and velocity distributions. It is noted that the shape of the nanoparticles have a great effect on the temperature profile. Platelet shaped nanoparticles are observed to have the lowest temperature profile for $Cu - Al_2O_3$ blood HNF, attributed to the higher surface area of the shape. Brick shaped nanoparticles cause the lowest velocity distribution as compared to other shapes. Changes in the thermal diffusivity, as influenced by the Prandtl number, can affect the velocity profile of a fluid. The Prandtl number has a significant impact on the velocity distribution, with higher values of the Prandtl number leading to an increase in velocity. Additionally, the Grashof number also influences the velocity profile, as higher Grashof numbers correspond to higher velocity profiles. It is also noted that higher values of the radiation parameter R lead to an increase in the temperature distribution. Overall, the $Cu - Al_2O_3$ blood HNF is noted to have a generally lower temperature profile, and higher velocity profile when

compared with Cu-blood NF. These findings provide evidence and support for the enhanced thermal performance of the HNFs; however, this comes with the drawback of increased viscous effects resulting from higher volume fractions. The impact of the magnetic parameter M and angle θ are also evident from the observations made and noted.

The research concludes that fractional derivatives serve as a useful tool in the analysis of complex fluid dynamics problems, offering practical applications in a variety of fields including engineering and medicine.

5.2 Future Scope

The Casson fluid model is adopted in this work to capture the non-Newtonian properties of blood as the base fluid. The nanoparticles considered are SWCNTs, MWCNTs, Copper(Cu), and Aluminium Oxide (Al_2O_3). We also consider the fluid to be flowing over a vertical plate. Consequently, the current study can be expanded in the following ways:

- The artery of the cardiovascular system are typically shaped in the form of cylinders. In future, this problem can be extended to cylindrical shape and curved cylinder instead of a plate.
- Models such as Herschel-Bulkely fluid model, Carreau and Carreau-Yasuda fluid model can be used to model blood since they describe the behavior of the viscosity of blood in different scenarios.
- Additional nanoparticles, such as Zinc Oxide (ZnO), Titanium Dioxide (TiO_2), and Silver (Ag), can be investigated to develop novel blood HNFs. These new formulations can be evaluated in comparison to the existing results, aiming to enhance the thermal properties of blood.
- We can also consider using ternary hybrid nanofluids, with the aim of further improving the thermal properties of hybrid nanofluids.
- New approaches for solving physics differential equation problems can be explored, such as the use of artificial intelligence tools e.g. Physics Informed Neural Networks (PINNs), which may give us new insights into fluid mechanics problems [69].

A. Appendix for Chapter 3

A.1 Values of Constants for equation 3.20

$$b_1 = \frac{\eta_2\beta}{\eta_1} \qquad b_2 = \frac{\eta_3\beta}{\eta_1} \qquad b_3 = \frac{\eta_4\beta}{\eta_1} \qquad b_4 = \frac{H\beta}{\eta_1}$$

$$B = b_1 MSin\theta + \frac{b_2}{\kappa} + b_0 s \quad C = b_4\left[\frac{sCos\phi_0 + kSin\phi_0}{k^2+s^2}\right] \quad D = b_3 Gr\frac{1}{s\sqrt{L}-1} \quad L = \frac{\eta_4 Pr}{\eta_5 R}\frac{s^{1-\beta}}{(1-\alpha s^{-\alpha})^{\gamma}}$$

A.2 Solution steps of Temperature profile

$$(\rho C_p)_{nf}\frac{\partial T}{\partial \xi} = -\frac{\partial q}{\partial \xi} \tag{A.1}$$

$$q = -\frac{4}{3}\frac{\sigma^*}{K^*}\frac{\partial T^4}{\partial \xi}k_{nf}$$

or rather

$$q = -\frac{16}{3}\frac{\sigma^* T_\infty^3}{K^*}\frac{\partial T}{\partial \xi}k_{nf}. \tag{A.2}$$

From the energy equation, we have that

$$\frac{(\rho C_p)_{nf}}{(\rho C_p)_f}(\rho C_p)_f\frac{\partial T}{\partial \xi} = -\frac{\partial q}{\partial \xi}.$$

It follows that

$$\eta_4(\rho C_p)_f\frac{\partial T}{\partial \xi} = -\frac{\partial q}{\partial \xi},$$

where $\eta_4 = (1-\phi) + \phi\frac{(\rho C_p)_s}{(\rho C_p)_f}$.
From the radiative heat flux, we have

$$q = -\frac{16}{3}\frac{\sigma^* T_\infty^3}{K^*}\frac{\partial T}{\partial \xi}\frac{k_{nf}}{k_f}k_f, \tag{A.3}$$

which gives us

$$q = -R\eta_5 k_f\frac{\partial T}{\partial \xi}, \tag{A.4}$$

where $\eta_5 = \frac{(1-\phi)+2\phi\frac{k_s}{k_s-k_f}ln\left(\frac{k_s-k_f}{2k_f}\right)}{(1-\phi)+2\phi\frac{k_s}{k_s-k_f}ln\left(\frac{k_s+k_f}{2k_f}\right)}$ and $R = -\frac{16\sigma^* T_\infty^3}{3K^*}$.

We apply the Prabhakar fractional approach here thus:

$$q = -R\eta_5 k_f \, {}^{C}\mathfrak{D}^{\gamma}_{\alpha,\beta,\gamma} \frac{\partial T}{\partial \xi}. \tag{A.5}$$

Taking the Laplace transform of (A.5), we get

$$\mathcal{L}\{q\} = \mathcal{L}\left\{-R\eta_5 k_f \, {}^{C}\mathfrak{D}^{\gamma}_{\alpha,\beta,\gamma} \frac{\partial T}{\partial \xi}\right\},$$

$$\overline{q} = -R\eta_5 k_f \left[-\left(s^{\beta}\left(1-\alpha s^{-\alpha}\right)^{\gamma}\right)\right] \frac{\partial \overline{T}}{\partial \xi}. \tag{A.6}$$

Taking the Laplace transformation of the energy equation, we get

$$s\overline{T}\eta_4 \left(\rho C_p\right)_f = -\frac{\partial \overline{q}}{\partial \xi}. \tag{A.7}$$

Equation (A.6) implies that

$$\frac{\partial \overline{q}}{\partial \xi} = -R\eta_5 k_f \left(s^{\beta}\left(1-\alpha s^{-\alpha}\right)^{\gamma}\right) \frac{\partial^2 T}{\partial \xi^2}. \tag{A.8}$$

Substituting (A.8) into (A.7), we get:

$$\eta_4 s\overline{T}\left(\rho C_p\right)_f = -R\eta_5 k_f \left(s^{\beta}\left(1-\alpha s^{-\alpha}\right)^{\gamma}\right) \frac{\partial^2 \overline{T}}{\partial \xi^2}.$$

Dividing by k_f gives

$$\eta_4 s\overline{T}\frac{\left(\rho C_p\right)_f}{k_f} = -R\eta_5 \left(s^{\beta}\left(1-\alpha s^{-\alpha}\right)^{\gamma}\right) \frac{\partial^2 \overline{T}}{\partial \xi^2},$$

or rather

$$\eta_4 s\overline{T} Pr = -R\eta_5 \left(s^{\beta}\left(1-\alpha s^{-\alpha}\right)^{\gamma}\right) \frac{\partial^2 \overline{T}}{\partial \xi^2}, \tag{A.9}$$

where $Pr = \frac{\left(\rho C_p\right)_f}{k_f}$ is the Prandtl Number.

Rewriting this, we get the homogeneous differential equation:

$$\frac{\partial^2 \overline{T}}{\partial \xi^2} - \frac{\eta_4 Pr}{\eta_5 R} \frac{s^{1-\beta}}{\left(1-\alpha s^{-\alpha}\right)^{\gamma}} = 0 \tag{A.10}$$

The characteristic polynomial of this differential equation is

$$r^2 - M = 0, \tag{A.11}$$

where $M = \frac{\eta_4 Pr}{\eta_5 R}\frac{s^{1-\beta}}{(1-\alpha s^{-\alpha})^{\gamma}}$. This has a solution $r_1 = -\sqrt{M}$ and $r_2 = +\sqrt{M}$.

So the general solution is given by

$$\overline{T} = C_1 e^{\xi\sqrt{M}} + C_2 e^{-\xi\sqrt{M}}. \tag{A.12}$$

Now, implementing the initial conditions:

- $T_{(\xi,t)} \to 0$ as $\xi \to \infty$ means that $C_1 = 0$.

Hence

$$\overline{T} = C_2 e^{-\xi\sqrt{M}}. \tag{A.13}$$

- $\overline{T}_{(0,s)} = C_2$. At the same time, $\frac{\partial \overline{T}}{\partial \xi} = -\sqrt{M}C_2 e^{-\xi\sqrt{M}}$. So $\frac{\partial \overline{T}}{\partial \xi}(at0) = -\sqrt{M}C_2$

Hence we have

$$-\sqrt{M}C_2 = -\left(\frac{1}{s} + \overline{T}_{(0,s)}\right) \tag{A.14}$$

or rather,

$$-\sqrt{M}C_2 = -\left(\frac{1}{s} + C_2\right). \tag{A.15}$$

Solving for C_2, we get

$$C_2 = \frac{1}{s(\sqrt{M}-1)}. \tag{A.16}$$

Therefore, the solution of the differential equation is

$$\overline{T} = \frac{1}{s\left(\sqrt{\frac{\eta_s Pr}{\eta_5 R}\frac{s^{1-\beta}}{(1-as^{-\alpha})^{\gamma}}} - 1\right)} e^{\sqrt{\frac{\eta_s Pr}{\eta_5 R}\frac{s^{1-\beta}}{(1-as^{-\alpha})^{\gamma}}}}. \tag{A.17}$$

A.3 Solution steps for Velocity Profile

Given the momentum equation

$$\rho_{nf}\frac{\partial v}{\partial t} = \mu_{nf}\left(1 + \frac{1}{\beta_0}\right)\frac{\partial^2 v}{\partial \xi^2} - \left(\sigma_{nf}B_0^2 Sin\theta + \frac{\mu_{nf}}{\kappa}\right)v + g\left(\rho B_T\right)_{nf}\left(T - T_\infty\right) + K_0 Cos\left(kt + \phi_0\right), \tag{A.18}$$

We multiply each thermophysical quatity by $1 = \frac{x_f}{x_f}$, where x_f is the corresponding base fluid thermophysical quantity, in this manner:

$$\left(\frac{\rho_{nf}}{\rho_f}\cdot\rho_f\right)\frac{\partial v}{\partial t}=\left(\frac{\mu_{nf}}{\mu_f}\cdot\mu_f\right)\left(1+\frac{1}{\beta_0}\right)\frac{\partial^2 v}{\partial\xi^2}-\left(\left(\frac{\sigma_{nf}}{\sigma_f}\cdot\sigma_f\right)B_0^2 Sin\theta + \left(\frac{\mu_{nf}}{\mu_f}\cdot\mu_{nf}\right)\frac{1}{\kappa}v+g\left(\rho B_T\right)_{nf}\left(T-T_\infty\right)+K_0 Cos\left(kt+\phi_0\right)$$

which leads us to

$$\eta_0\rho_f\frac{\partial v}{\partial t}=\eta_1\mu_f\left(1+\frac{1}{\beta_0}\right)\frac{\partial^2 v}{\partial\xi^2}-\left(\eta_2\sigma_f B_0^2 Sin\theta+\eta_1\frac{\mu_f}{\kappa}\right)v+\eta_3 g\left(\rho B_T\right)_f\left(T-T_\infty\right)+K_0 Cos\left(kt+\phi_0\right).$$

where $\eta_0=(1-\phi)+\phi\frac{\rho_s}{\rho_f}$, $\eta_1=\frac{1}{(1-\phi)^{2.5}}$, $\eta_2=1+\left\{3\left(\frac{\sigma_s}{\sigma_f}-1\right)\phi\right\}\left\{\left(\frac{\sigma_s}{\sigma_f}+1\right)-\left(\frac{\sigma_s}{\sigma_f}-1\right)\phi\right\}^{-1}$, $\eta_3=(1-\phi)+\phi\frac{(\rho B_T)_s}{(\rho B_T)_f}$, $\eta_4=(1-\phi)+\phi\frac{(\rho C_p)_s}{(\rho C_p)_f}$, $\eta_5=\frac{(1-\phi)+2\phi\frac{k_s}{k_s-k_f}ln\left(\frac{k_s-k_f}{2k_f}\right)}{(1-\phi)+2\phi\frac{k_s}{k_s-k_f}ln\left(\frac{k_s+k_f}{2k_f}\right)}$, Dividing throughout by ρ_f, we get

$$\eta_0\frac{\partial v}{\partial t}=\eta_1\frac{\mu_f}{\rho_f}\left(1+\frac{1}{\beta_0}\right)\frac{\partial^2 v}{\partial\xi^2}-\left(\frac{\eta_2\sigma_f B_0^2 Sin\theta}{\rho_f}+\frac{\eta_1\mu_f}{\kappa\rho_f}\right)v+\eta_3\frac{g\left(\rho B_T\right)_f\left(T-T_\infty\right)}{\rho_f}+\eta_4 K_0 Cos\left(kt+\phi_0\right). \tag{A.19}$$

We introduce the following non-dimensional variables:

$$v^*=\frac{v}{v_0},\quad \xi^*=\frac{v_0}{v_f}\xi,\quad t^*=\frac{v_0^2}{v_f}t,\quad T^*=\frac{T_{(\xi,t)}-T_\infty}{T_W-T_\infty},\quad q^*=\frac{q}{q_0},\quad q_0=k_f\frac{(T_W-T_\infty)v_0}{v_f}(fix)$$

Introducing these non-dimensional variables into equation (A.19), we obtain:

$$\eta_0\frac{v_0^3}{v_f}\frac{\partial v^*}{\partial t^*}=\eta_1\frac{1}{\beta_1}\frac{v_0^3}{v_f^2}\frac{\partial^2 v^*}{\partial\xi^{*2}}-\left(\frac{\eta_2\sigma_f B_0^2 Sin\theta}{\rho_f}+\frac{\eta_1}{\kappa}\right)v_0 v^* + \eta_3\frac{g\left(\rho B_T\right)_f\left(T_w-T_\infty\right)T^*+T_\infty-T_\infty}{\rho_f}+\eta_4 K_0 Cos\left(kt+\phi_0\right).$$

Multiplying throughout by $\frac{v_f}{v_0^3}$, we get:

$$\eta_0\frac{\partial v^*}{\partial t^*}=\frac{\eta_1}{\beta_1}\frac{\mu_f}{\rho_f}\frac{1}{v_f}\frac{\partial^2 v^*}{\partial\xi^{*2}}-\left(\frac{\eta_2\sigma_f B_0^2 Sin\theta}{\rho_f v_0^2}+\frac{\eta_1 v_f}{\kappa v_0^2}\right)v^*+\eta_3\frac{g\left(\rho B_T\right)_f\left(T_w-T_\infty\right)T^*}{\rho_f v_0^3}+\frac{\eta_4 v_f K_0}{v_0^3}Cos\left(kt+\phi_0\right).$$

$$\eta_0\frac{\partial v^*}{\partial t^*}=\frac{\eta_1}{\beta_1}\frac{\partial^2 v^*}{\partial\xi^{*2}}-\left(\eta_2 M Sin\theta+\frac{\eta_1}{K}\right)v^*+\eta_3 GrT^*+HCos\left(kt+\phi_0\right).$$

where $M = \frac{\sigma_f B_0^2 v_f}{\rho_f v_0^2}$, $Gr = \frac{g(\rho B_T)_f (T_w - T_\infty) T^*}{v_0^3}$, $H = \frac{\eta_4 K_0}{v_0^3}$, also keeping in mind that $v_f = \frac{\mu_f}{\rho_f}$.

Dropping the * sign for simplicity,

$$\eta_0 \frac{\partial v}{\partial t} = \frac{\eta_1}{\beta_1} \frac{\partial^2 v}{\partial \xi^2} - \left(\eta_2 MSin\theta + \frac{\eta_1}{K} \right) v + \eta_3 GrT + HCos\left(kt + \phi_0\right).$$

Now we take the Laplace transform of the above differential equation thus:

$$\mathcal{L}\left\{ \eta_0 \frac{\partial v}{\partial t} \right\} = \mathcal{L}\left\{ \frac{\eta_1}{\beta_1} \frac{\partial^2 v}{\partial \xi^2} - \left(\eta_2 MSin\theta + \frac{\eta_1}{K} \right) v + \eta_3 GrT + HCos\left(kt + \phi_0\right) \right\},$$

which gives us

$$\eta_0 s\overline{v} = \frac{\eta_1}{\beta_1} \frac{\partial^2 \overline{v}}{\partial \xi^2} - \left(\eta_2 MSin\theta + \frac{\eta_1}{K} \right) \overline{v} + \eta_3 Gr\overline{T} + H\left[\frac{sCos\phi_0 + kSin\phi_0}{k^2 + s^2} \right]. \tag{A.20}$$

Multiplying throughout by $\frac{\beta_1}{\eta_1}$,

$$\frac{\eta_0 \beta_1}{\eta_1} s\overline{v} = \frac{\partial^2 \overline{v}}{\partial \xi^2} - \left(\frac{\eta_2 \beta_1}{\eta_1} MSin\theta + \frac{\eta_3 \beta_1}{\eta_1} \frac{1}{K} \right) \overline{v} + \frac{\eta_4 \beta_1}{\eta_1} Gr\overline{T} + \frac{H\beta_1}{\eta_1} \left[\frac{sCos\phi_0 + kSin\phi_0}{k^2 + s^2} \right]. \tag{A.21}$$

By letting $b_0 = \frac{\eta_0 \beta_1}{\eta_1}$, $b_1 = \frac{\eta_2 \beta_1}{\eta_1}$, $b_2 = \frac{\eta_3 \beta_1}{\eta_1}$, $b_3 = \frac{\eta_4 \beta_1}{\eta_1}$ and $b_4 = \frac{H\beta_1}{\eta_1}$, the above differential equation simplifies to

$$b_0 s\overline{v} = \frac{\partial^2 \overline{v}}{\partial \xi^2} - \left(b_1 MSin\theta + \frac{b_2}{K} \right) \overline{v} + b_3 Gr\overline{T} + b_4 \left[\frac{sCos\phi_0 + kSin\phi_0}{k^2 + s^2} \right]. \tag{A.22}$$

Re-arranging this, we get:

$$\frac{\partial^2 \overline{v}}{\partial \xi^2} - \left(b_1 MSin\theta + \frac{b_2}{K} + b_0 s \right) \overline{v} + b_4 \left[\frac{sCos\phi_0 + kSin\phi_0}{k^2 + s^2} \right] = -b_3 Gr\overline{T}, \tag{A.23}$$

which is the equation to be solved.

By letting $A = 1$, $B = b_1 MSin\theta + \frac{b_2}{K} + b_0 s$, $C = b_4 \left[\frac{sCos\phi_0 + kSin\phi_0}{k^2 + s^2} \right]$, and $D = -b_3 Gr\overline{T}$, the above differential equation is simply

$$A\frac{\partial^2 \overline{v}}{\partial \xi^2} - B\overline{v} + C = D\overline{T}(\xi). \tag{A.24}$$

First we solve the homogeneous version of the differential equation,

$$A\frac{\partial^2 \overline{v}}{\partial \xi^2} - B\overline{v} + C = 0.$$

This has the general solution

$$\overline{v} = c_1 e^{\xi\sqrt{B}} + c_2 e^{-\xi\sqrt{B}} + \frac{C}{B}.$$

Now we find the solution of the non-homogeneuos differential equation.

Let

$\overline{v} = \eta_c e^{-\xi\sqrt{L}}$

$\overline{v}' = \eta_c \left(-\sqrt{L}\right) e^{-\xi\sqrt{L}},$

$\overline{v}' = \eta_c \left(L\right) e^{-\xi\sqrt{L}},$

where $L = \frac{\eta_s Pr}{\eta_5 R} \frac{s^{1-\beta}}{(1-as^{-\alpha})^{\gamma}}$.

Substituting into (A.24), we get

$\eta_c L e^{-\xi\sqrt{L}} - \eta_c B e^{-\xi\sqrt{L}} = D e^{-\xi\sqrt{L}}$
$\eta_c L - \eta_c B = D$
$\eta_c (L - B) = D$
$\eta_c = \frac{D}{L-B}$

Therefore,

$$\overline{v}_p = \left(\frac{D}{L-B}\right) e^{\sqrt{L}}. \tag{A.25}$$

And finally, the solution of the velocity equation is:

$$\overline{v} = c_1 e^{\xi\sqrt{B}} + c_2 e^{-\xi\sqrt{B}} + \frac{C}{B} + \left(\frac{D}{L-B}\right) e^{-\xi\sqrt{L}}. \tag{A.26}$$

Now we apply the initial conditions.

$$\overline{v} \to 0 \text{ as } \xi \to \infty$$

means that $c_1 = 0$.

$$v_{(0,s)} = \frac{p!}{s^{p+1}} = c_2 + \frac{C}{B} + \frac{D}{L-B}$$

$$c_2 = \frac{p!}{s^{p+1}} - \frac{C}{B} - \frac{D}{L-B}. \tag{A.27}$$

As a result, the final velocity solution is given by:

$$\overline{v} = \left(\frac{p!}{s^{p+1}} - \frac{C}{B} - \frac{D}{L-B}\right) e^{-\xi\sqrt{B}} + \left(\frac{C}{B} + \frac{D}{L-B}\right) e^{-\xi\sqrt{L}}. \tag{A.28}$$

****

B. Appendix for Chapter 4

B.1 Solution steps of Temperature profile

Given the equations

$$(\rho C_p)_{hnf} \frac{\partial T}{\partial \xi} = -\frac{\partial q}{\partial \xi} \tag{B.1}$$

$$q = -\frac{4}{3}\frac{\sigma^*}{K^*}\frac{\partial T^4}{\partial \xi} k_{nf}$$

or rather

$$q = -\frac{16}{3}\frac{\sigma^* T_\infty^3}{K^*}\frac{\partial T}{\partial \xi} k_{hnf}. \tag{B.2}$$

From the energy equation, we have that

$$\frac{(\rho C_p)_{hnf}}{(\rho C_p)_f} (\rho C_p)_f \frac{\partial T}{\partial \xi} = -\frac{\partial q}{\partial \xi}.$$

It then follows that

$$\eta_4 (\rho C_p)_f \frac{\partial T}{\partial \xi} = -\frac{\partial q}{\partial \xi},$$

where $\eta_4 = \frac{(\rho C_p)_{hnf}}{(\rho C_p)_f}$.
From the radiative heat flux, we have

$$q \approx -\frac{16}{3}\frac{\sigma^* T_\infty^3}{K^*}\frac{\partial T}{\partial \xi}\frac{k_{nf}}{k_f} k_f, \tag{B.3}$$

which gives us

$$q \approx -R\eta_5 k_f \frac{\partial T}{\partial \xi}, \tag{B.4}$$

where $\eta_5 = \dfrac{(1-\phi)+2\phi\frac{k_s}{k_s-k_f} ln\left(\frac{k_s-k_f}{2k_f}\right)}{(1-\phi)+2\phi\frac{k_s}{k_s-k_f} ln\left(\frac{k_s+k_f}{2k_f}\right)}$ and $R = -\frac{16\sigma^* T_\infty^3}{3K^*}$.

Now, we apply the Atangana-Baleanu fractional approach here thus:

$$q_{(\xi,t)} = -{}^{AB}\mathfrak{D}_t^\beta R\frac{\partial T}{\partial \xi}, \tag{B.5}$$

Taking the Laplace transform of (B.5), we get

$$\mathcal{L}\{q\} = \mathcal{L}\left\{-{}^{AB}\mathfrak{D}_t^{\beta} R\frac{\partial T}{\partial \xi}\right\}.$$

But

$$\mathcal{L}[{}^{AB}\mathfrak{D}_t^{\beta}] = \frac{s^{\beta}\mathcal{L}(h_{(\xi,t)}) - h_{(\xi,0)}}{(1-\beta)s^{\beta}+\beta}. \tag{B.6}$$

Therefore

$$\overline{q} = \frac{s^{\beta}\overline{T}}{(1-\beta)s^{\beta}+\beta} R\frac{\partial \overline{T}_{(\xi,t)}}{\partial \xi}, \tag{B.7}$$

and

$$\eta_4 Prs\overline{T}_{(\xi,t)} = -\eta_5\frac{\partial \overline{q}_{(\xi,t)}}{\partial \xi}, \tag{B.8}$$

where $Pr = \frac{(\rho C_p)_f}{k_f}$ is the Prandtl Number. Substituting B.7 into B.8, we get the homogeneous differential equation:

$$\frac{\partial^2 \overline{T}_{(\xi,t)}}{\partial \xi^2} - \frac{\eta_4 Pr}{\eta_5 R}\frac{s^{\beta}}{(1-\beta)s^{\beta}+\beta}\overline{T} = 0. \tag{B.9}$$

The characteristic polynomial of this differential equation is

$$r^2 - M = 0, \tag{B.10}$$

where $M = \frac{\eta_4 Pr}{\eta_5 R}\frac{s^{\beta}}{(1-\beta)s^{\beta}+\beta}$. This has a solution $r_1 = -\sqrt{M}$ and $r_2 = +\sqrt{M}$.

So the general solution is given by

$$\overline{T} = C_1 e^{\xi\sqrt{M}} + C_2 e^{-\xi\sqrt{M}}. \tag{B.11}$$

Now, implementing the initial conditions:

- $T_{(\xi,t)} \to 0$ as $\xi \to \infty$ means that $C_1 = 0$.
- $T_{(0,t)} = 1 \implies \overline{T}_{(0,s)} = \frac{1}{s}$. As such, $C_2 = \frac{1}{s}$.

Finally, we have the solution of the temperature profile as:

$$\overline{T} = \frac{1}{s}e^{-\xi\sqrt{\frac{\eta_4 Pr}{\eta_5 R}\frac{s^{\beta}}{(1-\beta)s^{\beta}+\beta}}}. \tag{B.12}$$

B.2 Solution steps of Velocity profile

The process for non dimensionalisation is similar to that of the velocity profile of Chapter 3.

So, given the dimensionless differential equation for momentum:

$$\eta_0 \frac{\partial v}{\partial t} = \frac{\eta_1}{B}\frac{\partial^2 v}{\partial \xi^2} - \left(\eta_2 MSin\theta + \frac{\eta_1}{k}\right) v + \eta_3 T_{(\xi,t)}. \tag{B.13}$$

We introduce the Atangana-Baleanu time fractional derivative

$$\eta_0 {}^{AB}\mathfrak{D}_t v_{(\xi,t)} = \frac{\eta_1}{B}\frac{\partial^2 v}{\partial \xi^2} - \left(\eta_2 MSin\theta + \frac{\eta_1}{k}\right) v + \eta_3 T_{(\xi,t)}. \tag{B.14}$$

Taking the Laplace transform of the above equation we get,

$$\eta_0 \mathcal{L}[{}^{AB}\mathfrak{D}_t v_{(\xi,t)}] = \frac{\eta_1}{B}\frac{\partial^2 \overline{v}}{\partial \xi^2} - \left(\eta_2 MSin\theta + \frac{\eta_1}{k}\right) \overline{v} + \eta_3 \overline{T}_{(\xi,t)}, \tag{B.15}$$

which gives us

$$\eta_0 \left[\frac{s^\beta \mathcal{L}(v_{(\xi,t)} - v_{(\xi,0)}}{(1-\beta)s^\beta + \beta}\right] = \frac{\eta_1}{B}\frac{\partial^2 \overline{v}}{\partial \xi^2} - \left(\eta_2 MSin\theta + \frac{\eta_1}{k}\right) \overline{v} + \eta_3 \overline{T}_{(\xi,t)}, \tag{B.16}$$

by definition of the Laplace of the Atangana-Baleanu time fractional derivative. Since $v_{(\xi,0)} = 0$ by the initial conditions, (B.16) becomes:

$$\eta_0 \left[\frac{s^\beta \overline{v}_{(\xi,t)}}{(1-\beta)s^\beta + \beta}\right] = \frac{\eta_1}{B}\frac{\partial^2 \overline{v}}{\partial \xi^2} - \left(\eta_2 MSin\theta + \frac{\eta_1}{k}\right) \overline{v} + \eta_3 \overline{T}_{(\xi,t)}. \tag{B.17}$$

Dividing throughout by $\frac{\eta_1}{B}$, and rearranging, we get:

$$\frac{\partial^2 \overline{v}_{(\xi,s)}}{\partial \xi^2} - \left(\frac{l_4 s^\beta + l_5}{s^\beta + l_2}\right) \overline{v}_{(\xi,s)} = -\eta_3 \overline{T}_{(\xi,s)}. \tag{B.18}$$

Solving the homogeneous equation first,

$$\frac{\partial^2 \overline{v}_{(\xi,s)}}{\partial \xi^2} - \left(\frac{l_4 s^\beta + l_5}{s^\beta + l_2}\right) \overline{v}_{(\xi,s)} = 0. \tag{B.19}$$

Characteristic polynomial is $r^2 - Q = 0$, where $Q = \frac{l_4 s^\beta + l_5}{s^\beta + l_2}$

Therefore the general solution is:

$$\overline{v}_{(\xi,s)} = C_1 e^{\xi\sqrt{Q}} + C_2 e^{-\xi\sqrt{Q}}. \tag{B.20}$$

The particular solution of B.18 is

$$\overline{v}_p = \frac{1}{s}\left(\frac{-b_3}{M+Q}\right)e^{-\xi\sqrt{M}} \tag{B.21}$$

Hence the solution is given by:

$$\overline{v}_{(\xi,s)} = C_1 e^{\xi\sqrt{Q}} + C_2 e^{-\xi\sqrt{Q}} + \frac{1}{s}\left(\frac{-b_3}{M+Q}\right)e^{-\xi\sqrt{M}}. \tag{B.22}$$

Now implementing the initial conditions,

- $\overline{v} \to 0$, therefore $C_1 = 0$
- $v_{(0,t)} = H(t)Cos(\omega t)$, so $\overline{v}_{(0,t)} = \frac{s}{s^2+\omega^2}$. Therefore $C_2 = \frac{s}{s^2+\omega^2}$

After rearranging, we get the solution:

$$\overline{v}_{(\xi,s)} = \frac{s}{s^2+\omega^2}e^{-\sqrt{\frac{l_4 s^\beta + l_5}{s^\beta + l_2}}} + \frac{l_3(s^\beta + l_2)}{s((l_1 - l_4)s^\beta - l_5)}\left(e^{-\xi\sqrt{\frac{l_4 s^\beta + l_5}{s^\beta + l_2}}} - e^{-\xi\sqrt{\frac{l_1 s^\beta}{s^\beta + l_2}}}\right). \tag{B.23}$$

Bibliography

[1] U. S. Dixit, M. Hazarika, and J. P. Davim, *History of Thermodynamics and Heat Transfer*, pp. 73–97. Cham: Springer International Publishing, 2017.

[2] Wikimedia, "Rheology of time independent fluids," 2023.

[3] N. Özkaya, D. Leger, D. Goldsheyder, and M. Nordin, *Multiaxial Deformations and Stress Analyses*, pp. 317–360. Cham: Springer International Publishing, 2017.

[4] N. Casson, "A flow equation for pigment-oil suspensions of the printing ink type," *Rheology of disperse systems*, 1959.

[5] M. Caputo, "Linear Models of Dissipation whose Q is almost Frequency Independent—II," *Geophysical Journal International*, vol. 13, pp. 529–539, 11 1967.

[6] M. Caputo and M. Fabrizio, "A new definition of fractional derivative without singular kernel," *Prog Fract Differ Appl*, vol. 1, pp. 73–85, 04 2015.

[7] A. Atangana, "New fractional derivatives with nonlocal and non-singular kernel: Theory and application to heat transfer model," *Thermal Science*, vol. 20, 01 2016.

[8] T. R. Prabhakar, "A singular integral equation with a generalized mittag-leffler function in the kernel," *Yokohama math. J*, vol. 19, no. 1, pp. 7–15, 1971.

[9] L. Debnath, "Recent applications of fractional calculus to science and engineering.," *International Journal of Mathematics and Mathematical Sciences*, vol. 2003, no. 54, pp. 3413–3442, 2003.

[10] S. Mobasser and A. A. Firoozi, "Review of nanotechnology applications in science and engineering," vol. 6, pp. 84–93, 07 2016.

[11] A. Prasad, S. Singh, and H. Nagar, "A review on nanofluids: Properties and applications," *International Journal Of Advance Research And Innovative Ideas In Education*, vol. 3, pp. 3185–3209, 01 2017.

[12] S. Choi and J. A. Eastman, "Enhancing thermal conductivity of fluids with nanoparticles," tech. rep., Argonne National Lab.(ANL), Argonne, IL (United States), 1995.

[13] Y. Khan, H. Sadia, S. Z. Ali Shah, M. N. Khan, A. A. Shah, N. Ullah, M. F. Ullah, H. Bibi, O. T. Bafakeeh, N. B. Khedher, S. M. Eldin, B. M. Fadhl, and M. I. Khan, "Classification, synthetic, and characterization approaches to nanoparticles, and their applications in various fields of nanotechnology: A review," *Catalysts*, vol. 12, no. 11, 2022.

[14] K. Wong and O. Leon, "Applications of nanofluids: Current and future," *Advances in Mechanical Engineering*, vol. 2, 01 2010.

[15] S. Shaw, G. Mahanta, and P. Sibanda, "Non-linear thermal convection in a casson fluid flow over a horizontal plate with convective boundary condition," *Alexandria Engineering Journal*, vol. 55, no. 2, pp. 1295–1304, 2016.

[16] N. N. Kumar, D. Sastry, and S. Shaw, "Irreversibility analysis of an unsteady micropolar cnt-blood nanofluid flow through a squeezing channel with activation energy-application in drug delivery," *Computer Methods and Programs in Biomedicine*, vol. 226, p. 107156, 2022.

[17] A. Saeed, A. Alsubie, P. Kumam, S. Nasir, T. Gul, and W. Kumam, "Blood based hybrid nanofluid flow together with electromagnetic field and couple stresses," *Scientific Reports*, vol. 11, p. 12865, Jun 2021.

[18] S. K. Sahu, S. Shaw, D. N. Thatoi, and M. K. Nayak, "A thermal management of darcy-forchheimer swcnt–mwcnt cross hybrid nanofluid flow due to vertical stretched cylinder with and without inertia effects," *Waves in Random and Complex Media*, vol. 0, no. 0, pp. 1–27, 2022.

[19] S. Noreen, M. M. Rashidi, and M. Qasim, "Blood flow analysis with considering nanofluid effects in vertical channel," *Applied Nanoscience*, vol. 7, pp. 193–199, Jun 2017.

[20] Z. Shah, A. Khan, W. Khan, M. Kamran Alam, S. Islam, P. Kumam, and P. Thounthong, "Micropolar gold blood nanofluid flow and radiative heat transfer between permeable channels," *Computer Methods and Programs in Biomedicine*, vol. 186, p. 105197, 2020.

[21] M. H. Esfe, R. Dalir, R. Bakhtiari, and M. Afrand, "Simultaneous effects of multi-walled carbon nanotubes and copper oxide nanoparticles on the rheological behavior of cooling oil: Application for refrigeration systems," *International Journal of Refrigeration*, vol. 104, pp. 123–133, 2019.

[22] S. Samanta and R. R. Sahoo, "Covalently linked hexagonal boron Nitride-Graphene oxide nanocomposites as High-Performance Oil-Dispersible lubricant additives," *ACS Appl. Nano Mater.*, vol. 3, pp. 10941–10953, Nov. 2020.

[23] H. Pourpasha, S. Zeinali Heris, and M. Mohammadpourfard, "The effect of tio2 doped multi-walled carbon nanotubes synthesis on the thermophysical and heat transfer properties of transformer oil: A comprehensive experimental study," *Case Studies in Thermal Engineering*, vol. 41, p. 102607, 2023.

[24] G. Paul, J. Philip, B. Raj, P. K. Das, and I. Manna, "Synthesis, characterization, and thermal property measurement of nano-al95zn05 dispersed nanofluid prepared by a two-step process," *International Journal of Heat and Mass Transfer*, vol. 54, no. 15, pp. 3783–3788, 2011.

[25] F. Jamil and H. M. Ali, "Chapter 6 - applications of hybrid nanofluids in different fields," in *Hybrid Nanofluids for Convection Heat Transfer* (H. M. Ali, ed.), pp. 215–254, Academic Press, 2020.

[26] M. Nayak, S. Shaw, H. Waqas, O. Makinde, M. Alghamdi, and T. Muhammad, "Comparative study for magnetized flow of nanofluids between two parallel permeable stretching/shrinking surfaces," *Case Studies in Thermal Engineering*, vol. 28, p. 101353, 2021.

[27] S. Shaw, A. S. Dogonchi, M. K. Nayak, and O. D. Makinde, "Impact of entropy generation and nonlinear thermal radiation on darcy–forchheimer flow of mnfe2o4-casson/water nanofluid due to a rotating disk: Application to brain dynamics," *Arabian Journal for Science and Engineering*, vol. 45, pp. 5471–5490, July 2020.

[28] W. Alghamdi, T. Gul, M. Nullah, A. Rehman, S. Nasir, A. Saeed, and E. Bonyah, "Boundary layer stagnation point flow of the casson hybrid nanofluid over an unsteady stretching surface," *AIP Advances*, vol. 11, no. 1, p. 015016, 2021.

[29] A. Saeed, N. Khan, T. Gul, W. Kumam, W. Alghamdi, and P. Kumam, "The flow of blood-based hybrid nanofluids with couple stresses by the convergent and divergent channel for the applications of drug delivery," *Molecules*, vol. 26, p. 23, 10 2021.

[30] H. Nakamura, T. Okazawa, H. Nagase, M. Yoshida, M. Arüzumi, and A. Okada, "Change in digital blood flow with simultaneous reduction in plasma endothelin induced by hand-arm vibration," *International Archives of Occupational and Environmental Health*, vol. 68, pp. 115–119, Jan. 1996.

[31] S. Maiti, S. Shaw, and G. Shit, "Fractional order model for thermochemical flow of blood with dufour and soret effects under magnetic and vibration environment," *Colloids and Surfaces B: Biointerfaces*, vol. 197, p. 111395, 2021.

[32] S. Kadhim, M. Nasif, H. Al-Kayiem, T. Nagarajan, and R. Al-Waked, "Effect of induced vibration on the blood flow properties in a mechanical aortic valve," *MATEC Web of Conferences*, vol. 13, p. 02022, 07 2014.

[33] S. Akcay, U. Akdag, and H. Palancioglu, "Experimental investigation of mixed convection on an oscillating vertical flat plate," *International Communications in Heat and Mass Transfer*, vol. 113, p. 104528, 2020.

[34] F. Ali, I. Khan, and S. Shafie, "Closed form solutions for unsteady free convection flow of a second grade fluid over an oscillating vertical plate," *PLoS One*, vol. 9, p. e85099, Feb. 2014.

[35] N. A. Shah and I. Khan, "Heat transfer analysis in a second grade fluid over and oscillating vertical plate using fractional caputo–fabrizio derivatives," *The European Physical Journal C*, vol. 76, p. 362, Jul 2016.

[36] B. Shankar Goud, P. Srilatha, T. Srinivasulu, Y. Dhamendar Reddy, and K. Sandeep Kumar, "Induced by heat source on unsteady mhd free convective flow of casson fluid past a vertically oscillating plate through porous medium utilizing finite difference method," *Materials Today: Proceedings*, 2023.

[37] H. I. Abdel-Gawad, "Dynamics of steady, unsteady flows and heat transfer in casson fluid over a free stretching surface: stability analysis," *Waves in Random and Complex Media*, pp. 1–19, 2023.

[38] A. K. Jagadeesan, K. Thangavelu, and V. Dhananjeyan, "Carbon nanotubes: Synthesis, properties and applications," in *21st Century Surface Science* (P. Pham, P. Goel, S. Kumar, and K. Yadav, eds.), ch. 2, Rijeka: IntechOpen, 2020.

[39] A. Venkataraman, E. V. Amadi, Y. Chen, and C. Papadopoulos, "Carbon nanotube assembly and integration for applications," *Nanoscale Research Letters*, vol. 14, p. 220, July 2019.

[40] N. Anzar, R. Hasan, M. Tyagi, N. Yadav, and J. Narang, "Carbon nanotube - a review on synthesis, properties and plethora of applications in the field of biomedical science," *Sensors International*, vol. 1, p. 100003, 01 2020.

[41] T. Gul, R. S. Gul, W. Noman, A. Saeed, S. Mukhtar, W. Alghamdi, and H. Alrabaiah, "Cnts-nanofluid flow in a rotating system between the gap of a disk and cone," *Physica Scripta*, vol. 95, p. 125202, oct 2020.

[42] Y. Wang, I. B. Mansir, K. Al-Khaled, A. Raza, S. U. Khan, M. I. Khan, and A. El-Sayed Ahmed, "Thermal outcomes for blood-based carbon nanotubes (swcnt and mwcnts) with newtonian heating by using new prabhakar fractional derivative simulations," *Case Studies in Thermal Engineering*, vol. 32, p. 101904, 2022.

[43] S. E. Ahmed, "Caputo fractional convective flow in an inclined wavy vented cavity filled with a porous medium using al2o3-cu hybrid nanofluids," *International Communications in Heat and Mass Transfer*, vol. 116, p. 104690, 2020.

[44] S. Ijaz and S. Nadeem, "Shape factor and sphericity features examination of cu and cu-al2o3/blood through atherosclerotic artery under the impact of wall characteristic," *Journal of Molecular Liquids*, vol. 271, pp. 361–372, 2018.

[45] W. Alghamdi, A. Alsubie, P. Kumam, A. Saeed, and T. Gul, "Mhd hybrid nanofluid flow comprising the medication through a blood artery," *Scientific Reports*, vol. 11, no. 1, p. 11621, 2021.

[46] M. Yasir, Z. U. Malik, A. K. Alzahrani, and M. Khan, "Study of hybrid al2o3-cu nanomaterials on radiative flow over a stretching/shrinking cylinder: Comparative analysis," *Ain Shams Engineering Journal*, vol. 14, no. 9, p. 102070, 2023.

[47] M. Yavuz and N. Özdemir, "Comparing the new fractional derivative operators involving exponential and mittag-leffler kernel," *Discrete and Continuous Dynamical Systems - S*, vol. 13, no. 3, pp. 995–1006, 2020.

[48] R. Garra and R. Garrappa, "The prabhakar or three parameter mittag–leffler function: Theory and application," *Communications in Nonlinear Science and Numerical Simulation*, vol. 56, pp. 314–329, 2018.

[49] M. Asjad, M. Zahid, Y. Chu, and D. Baleanu, "Prabhakar fractional derivative and its applications in the transport phenomena containing nanoparticles," *Thermal Science*, vol. 25, pp. 1–6, 11 2021.

[50] F. Wang, M. I. Asjad, M. Zahid, A. Iqbal, H. Ahmad, and M. Alsulami, "Unsteady thermal transport flow of casson nanofluids with generalized mittag–leffler kernel of prabhakar's type," *Journal of Materials Research and Technology*, vol. 14, pp. 1292–1300, 2021.

[51] Z. Jie, M. Khan, K. Al-Khaled, E. El-Zahar, N. Acharya, A. Raza, S. Khan, W.-F. Xia, and N.-x. Tao, "Thermal transport model for brinkman type nanofluid containing carbon nanotubes with sinusoidal oscillations conditions: a fractional derivative concept," *Waves in Random and Complex Media*, pp. 1–20, 03 2022.

[52] A. Raza, K. Al-Khaled, M. I. Khan, S. Farid, S. U. Khan, S. I. Shah, and R. Ali, "Investigation of dynamics of swcnts and mwcnts nanoparticles in blood flow using the atangana–baleanu time fractional derivative with ramped temperature," *Proceedings of the Institution of Mechanical Engineers, Part E: Journal of Process Mechanical Engineering*, p. 09544089211047747, Oct 2021.

[53] E. V. Timofeeva, J. L. Routbort, and D. Singh, "Particle shape effects on thermophysical properties of alumina nanofluids," *Journal of applied physics*, vol. 106, no. 1, p. 014304, 2009.

[54] D. Tripathi, J. Prakash, A. K. Tiwari, and R. Ellahi, "Thermal, microrotation, electromagnetic field and nanoparticle shape effects on cu-cuo/blood flow in microvascular vessels," *Microvascular Research*, vol. 132, p. 104065, 2020.

[55] D. Y. Tzou, *Macro-to microscale heat transfer: the lagging behavior*. John Wiley & Sons, 2014.

[56] V. Zakian and R. K. Littlewood, "Numerical inversion of Laplace transforms by weighted least-squares approximation," *The Computer Journal*, vol. 16, pp. 66–68, 01 1973.

[57] M. Q. Brewster, *Thermal radiative transfer and properties*. John Wiley & Sons, 1992.

[58] D. Halsted and D. Brown, "Zakian's technique for inverting laplace transforms," *The Chemical Engineering Journal*, vol. 3, pp. 312–313, 1972.

[59] T. M. Inc., "Matlab version: 9.13.0 (r2022b)," 2022.

[60] A. Raza, U. Khan, A. Zaib, E. E. Mahmoud, W. Weera, I. S. Yahia, and A. M. Galal, "Applications of prabhakar-like fractional derivative for the solution of viscous type fluid with newtonian heating effect," *Fractal and Fractional*, vol. 6, no. 5, 2022.

[61] A. Basit, M. Asjad, and A. Akgül, "Convective flow of a fractional second grade fluid containing different nanoparticles with prabhakar fractional derivative subject to non-uniform velocity at the boundary," *Mathematical Methods in the Applied Sciences*, vol. 46, May 2021.

[62] T. Elnaqeeb, N. A. Shah, and I. A. Mirza, "Natural convection flows of carbon nanotubes nanofluids with prabhakar-like thermal transport," *Mathematical Methods in the Applied Sciences*, 2020.

[63] U. Majeed, M. I. Asjad, M. I. Qadir, and A. Akgül, "Effect of slip on generalized viscous nanofluid with thermal flux with effective fractional derivative," 2022.

[64] M. Shen, H. Chen, M. Zhang, F. Liu, and V. Anh, "A comprehensive review of nanofluids with fractional derivatives: Modeling and application," *Nanotechnology Reviews*, vol. 11, no. 1, pp. 3235–3249, 2022.

[65] H. Sheng, Y. Li, and Y. Chen, "Application of numerical inverse laplace transform algorithms in fractional calculus," *Journal of the Franklin Institute*, vol. 348, no. 2, pp. 315–330, 2011.

[66] D. Halsted and D. Brown, "Zakian's technique for inverting laplace transforms," *The Chemical Engineering Journal*, vol. 3, pp. 312–313, 1972. An International Journal of Research and Development.

[67] N. Saeed, N. Sarwar, and A. Riaz, "The mhd effect on a fractional casson nanofluid with constant boundary conditions and the generalized mittag-leffler kernel," *Comput. J. Comb. Math*, vol. 3, pp. 11–22, 2021.

[68] Y. Wang, A. Raza, S. U. Khan, M. I. Khan, M. Ayadi, M. A. El-Shorbagy, N. A. Alshehri, F. Wang, and M. Y. Malik, "Prabhakar fractional simulations for hybrid nanofluid with aluminum oxide, titanium oxide and copper nanoparticles along with blood base fluid," *Waves in Random and Complex Media*, vol. 0, no. 0, pp. 1–20, 2022.

[69] S. Cai, Z. Mao, Z. Wang, M. Yin, and G. E. Karniadakis, "Physics-informed neural networks (pinns) for fluid mechanics: a review," *Acta Mechanica Sinica*, vol. 37, pp. 1727–1738, Dec 2021.

[70] J. Ndenda, J. Njagarah, and S. Shaw, "Role of immunotherapy in tumor-immune interaction: Perspectives from fractional-order modelling and sensitivity analysis," *Chaos, Solitons Fractals*, vol. 148, p. 111036, 2021.

[71] H. B. Yadeta and S. Shaw, "Magnetic drug targeting during casson blood flow in a microvessel: A caputo fractional model," *Journal of Magnetism and Magnetic Materials*, vol. 568, p. 170363, 2023.

[72] F. Polito and Z. Tomovski, "Some properties of prabhakar-type fractional calculus operators," *arXiv preprint arXiv:1508.03224*, 2015.

[73] A. Giusti and I. Colombaro, "Prabhakar-like fractional viscoelasticity," *Communications in Nonlinear Science and Numerical Simulation*, vol. 56, pp. 138–143, 2018.

[74] G. E. Miller, "Chapter 14 - biomedical transport processes," in *Introduction to Biomedical Engineering (Third Edition)*, Biomedical Engineering, pp. 937–993, Boston: Academic Press, third edition ed., 2012.